

# Robust formation of metachronal waves in directional chains of phase oscillators

A. C. Quillen<sup>1,\*</sup>

<sup>1</sup>*Department of Physics and Astronomy, University of Rochester, Rochester, NY 14627, USA*

Biological systems can rely on collective formation of a metachronal wave in an ensemble of oscillators for locomotion and for fluid transport. We consider one-dimensional chains of phase oscillators with nearest neighbor interactions, connected in a loop and with rotational symmetry, so each oscillator resembles every other oscillator in the chain. Numerical integrations of the discrete phase oscillator systems and a continuum approximation show that directional models (those that do not obey reversal symmetry), can exhibit instability to short wavelength perturbations but only in regions where the slope in phase has a particular sign. This causes short wavelength perturbations to develop that can vary the winding number that describes the sum of phase differences across the loop and the resulting metachronal wave speed. Numerical integrations of stochastic directional phase oscillator models show that even a weak level of noise can seed instabilities that resolve into metachronal wave states.

## I. INTRODUCTION

Models of interacting phase oscillators, such as the Kuramoto model, have been used to study the dynamics of synchronization in a wide variety of physical and biological systems [1–5]. The head or tail of an individual flagellum, cilium or nematode moves back and forth with respect to a mean position. This periodic motion can be described with a phase of oscillation, with the collective behavior of the system governed by interactions between neighboring individual bodies. When the interactions are strong, all oscillators can lock in phase and beat together in a globally synchronized pattern. A metachronal rhythm or metachronal wave refers to a collective state where individuals are undergoing periodic motions but synchronization is only local. The motions of each individual is the same as that of their neighbors but there is a delay between these motions, giving the appearance of a traveling wave.

Perhaps the most common example of emergent traveling waves are in ciliary carpets. Hydrodynamic interactions between actively beating cilia, spontaneously result in the formation of large-scale metachronal waves [6]. Such organized waves are critical for the motility of ciliated protists (such as the *Paramecium* [7]), mucus clearance in mammalian airways [8, 9], and for fluid transport in the brain [10]. Metachronal waves can also form in concentrations of swimming nematodes [11] where they can be mediated by steric interactions [12].

What fraction of possible initial conditions would converge onto a wave-like solution? The set of initial conditions that converge onto a particular solution are called its *basin of attraction*. In many models of interacting phase oscillators, the basins of attraction for traveling wave solutions are smaller than that of the synchronous state [13–15]. In other words, using an ensemble of random generated initial phases for each phase oscillator, a system would be more likely to enter a synchronous

rather than a traveling wave state.

Because many well studied models are more likely to enter a synchronous than a traveling wave state, or produce waves traveling in either direction, they do not capture the behavior illustrated by vinegar eels [11, 12], or other systems that exhibit metachronal waves, such as chains of cilia [16], cilia carpets [17] or flagella on the surface of *Volvox carteri* alga colonies [18]. Relevant models for these types of biological systems should exhibit a larger basin of attraction for traveling wave states than for the synchronous state. Recently Chakrabarti et al. [6] showed that that in the continuum limit, interactions between cilia in a one dimensional loop lead to conservation of a type of topological charge or a winding number. The conserved quantity implies that initial conditions could set the wave speed of attracting solutions. To mitigate the role of the constraint imposed by the conserved quantity, Chakrabarti et al. [6] proposed that irregularities or gaps in the spacing between cilia could help account for systems of cilia that robustly exhibit metachronal waves.

A model with asymptotic behavior dependent upon initial conditions is inconvenient when trying to model biological systems. However, fluctuations are likely to be present in ciliated systems (e.g., [19]). The presence of noise could affect or even determine the statistics of long-lived states, obviating the need to understand the sensitivity to initial conditions. When coupled to a phase oscillator model for ciliated carpets, white noise can cause stochastic transitions between synchronized states and disordered states [17].

The focus of this manuscript is to explore properties of interacting phase oscillator systems that allow them to robustly enter wave-like states. Building upon the work by Chakrabarti et al. [6], we investigate if and how model systems can exhibit changes in the winding number. In section IA we describe states for systems of interacting phase oscillators. In section IB and IC we introduce chains of interacting oscillators and describe what we mean by a directional model. In section ID we define how we calculate the phase shift between neighboring oscillators (following [15]) and the winding number. In section II we find a partial differential equation

\* alice.quillen@rochester.edu

that represents the continuum limit for a loop of oscillators with nearest neighbor interactions. The properties of the associated continuum equations are relevant for interpretation of our numerical integrations. In section III we numerically explore bidirectional, unidirectional and adjustable directional models to better understand how these models exhibit changes in winding number. In this section we use initial conditions that are either sinusoidal or drawn from a uniform distribution. In section IV and following Solovov and Friedrich [17] who found that noise could affect the coherence of wave-like states in ciliary carpets, we explore numerically adjustable directional models that are perturbed by white noise. We numerically explore how initial winding number and the number oscillators affect the integrated mean phase shift between neighboring oscillators and the standard deviation of the phase shifts. A summary and discussion follows in section V.

### A. Types of states for ensembles of phase oscillators

We denote each phase oscillator with a non-negative integer  $i$ . The  $i$ -th oscillator can be described with a phase  $\theta_i \in [0, 2\pi)$  that is a function of time  $t$  and a frequency of oscillation or a phase velocity  $\frac{d\theta_i}{dt} = \dot{\theta}_i = \omega_i$ .

Collective phenomena of an ensemble of interacting phase oscillators has been described with different nomenclature. Following [16, 20], a *synchronized* state of an ensemble of  $N$  oscillators is one where all oscillators have identical phases.

Synchronized:

$$\theta_i(t) = \theta_j(t) \text{ for all } i, j \in (0, 1, \dots, N-1). \quad (1)$$

A *phase-locked* or *frequency synchronized* state [21–23] is one where all oscillators have identical phase velocities

Phase-locked

$$\dot{\theta}_i(t) = \dot{\theta}_j(t) \text{ for all } i, j \in (0, 1, \dots, N-1). \quad (2)$$

Pairs of oscillators differ by a constant phase difference.

In a periodic *entrained* state, if the oscillators have identical mean or average phase velocities we call the state *entrained*;

Entrained:

$$\tilde{\omega}_i = \tilde{\omega}_j \text{ for all } i, j \in (0, 1, \dots, N-1). \quad (3)$$

For a periodic state with period  $T$ , the phases satisfy  $\theta_i(t+T) = \theta_i$  for all  $i$ . The average phase velocity  $\tilde{\omega}_i$  can be computed with an integral over the period  $T$ ,  $\tilde{\omega}_i = \frac{1}{T} \int_0^T \dot{\theta}_i(t) dt$ .

For a chain of oscillators, the index  $i$  specifies the order in the chain. One type of traveling wave is a *non-synchronous and phase-locked state* characterized by a

constant phase delay or offset between consecutive oscillators in a chain or loop of oscillators. In other words

Constant phase delay:

$$\theta_{i+1} = \theta_i + \phi \quad (4)$$

for consecutive oscillators, where  $\phi$  is called the phase delay, phase shift or phase difference and  $\dot{\theta}_i \neq 0$  for all  $i$ . If individual oscillators undergo similar periodic motions, then another type of traveling wave is a *non-synchronous and entrained state* characterized by a time delay between the motions of consecutive oscillators. In other words

Constant time delay:

$$\theta_i(t + \tau) = \theta_{i+1}(t) \quad (5)$$

with time delay  $\tau$ . In this case the phase velocities need not be constant. Both types of traveling waves involve periodic oscillator motions and are known in the literature as metachronal waves (e.g., [6, 12, 18, 24]).

### B. Local Kuramoto models

The Kuramoto model [2, 3, 20] consists of  $N$  phase oscillators, that mutually interact via a sinusoidal interaction term

$$\frac{d\theta_i}{dt} = \omega_{i,0} + \sum_{j=1}^N K_{ij} \sin(\theta_j - \theta_i) \quad (6)$$

where  $K_{ij}$  are non-negative coefficients giving the strength of the interaction between a pair of oscillators. Here  $i \in 0, 1, 2, \dots, N-1$  and each angle  $\theta_i \in [0, 2\pi]$ . In the absence of interaction, the  $i$ -th oscillator would have a constant phase velocity  $\omega_{i,0}$  which is called its intrinsic frequency. The intrinsic frequencies for each oscillator need not be identical.

With only nearest neighbor interactions, a well studied model, sometimes called a local Kuramoto model, is described by

$$\frac{d\theta_i}{dt} = \omega_{i,0} + K [\sin(\theta_{i+1} - \theta_i) + \sin(\theta_{i-1} - \theta_i)] \quad (7)$$

[14, 15, 21–23, 25]. Each oscillator only interacts with its nearest neighbors. At low values of positive interaction parameter  $K$ , the oscillators are not affected by their neighbors. At higher  $K$ , the oscillators cluster in phase velocity, and the number of clusters decreases until they fuse into a single cluster that spans the system. At and above a critical value of  $K = K_s$  the entire system must enter a global phase-locked state [26]. Above the critical value  $K > K_s$ , there can be multiple stable phase-locked attractors, each with its own value of global rotation rate  $\Omega = \frac{1}{N} \sum_i \omega_i$  [14, 27].

Instead of considering chains of oscillators that have different intrinsic frequencies, ( $\omega_{i,0} \neq \omega_{j,0}$  for  $i \neq j$ ) a

number of studies have focused on chains that have *rotational symmetry*. In these systems, each oscillator has the same equation of motion as the previous oscillator in the chain, but with index shifted by 1. For example, Tilles et al. [14], Dénes et al. [15], Niedermayer et al. [16] studied loops with nearest neighbor interactions. We refer to a chain of  $N$  phase oscillators that has a periodic boundary condition,  $\theta_0 = \theta_N$ ,  $\theta_{N+1} = \theta_1$ , as a *loop*.

For loops with rotationally symmetric interactions and identical intrinsic frequencies [15] the linearized system (linearized about a stable synchronous or phase-locked state) has Jacobian that is a circulant matrix. (This is a matrix where each row is a cyclic permutation of the previous row). This gives a closed form for the eigenvalues, which can be used to study the stability of synchronous or phase locked states (e.g., [16]). Ottino-Löffler and Strogatz [28] considered chains and loops of nearest neighbor coupled oscillators that differ in intrinsic or natural oscillator frequency. They found that for both topologies, stable phase-locked states exist if and only if the spread or ‘width’ of the natural frequencies is smaller than a critical value called the locking threshold. By studying a system with the coupling strength of a given link varies from zero (a chain with free ends) to one with a periodic boundary (a ring), Tilles et al. [14] investigated the birth of phase locked solutions.

### C. Loops of identical oscillators – rotational symmetry

We consider the class of loop systems that has only nearest neighbor interactions,

$$\frac{d\theta_i}{dt} = \omega_0 + H_+(\theta_i, \theta_{i+1}) + H_-(\theta_i, \theta_{i-1}) \quad (8)$$

which is rotationally symmetric because each oscillator resembles every other oscillator in the loop. Here intrinsic oscillator frequencies are the same for each oscillator and equal to  $\omega_0$ . The functions  $H_+$  and  $H_-$  are periodic in both arguments so  $H_+(\psi_1 + 2\pi, \psi_2) = H_+(\psi_1, \psi_2 + 2\pi) = H_+(\psi_1, \psi_2)$  and similarly for  $H_-()$ . Because we don’t specify the functions  $H_+, H_-$ , the model is more general than the local Kuramoto model (Eqn. 7) with sinusoidal interactions, and where all oscillators have the same intrinsic frequency ( $\omega_{i,0} = \omega_0$  for all  $i$ ).

The dynamical system of Eqn. 8 need not be symmetric to inversion ( $j \rightarrow N - 1 - j$  for  $j = 0, \dots, N - 1$ ), also known as *mirror symmetry* [17]. Equivalently, we need not require that the function  $H_+()$  be the same as  $H_-()$ . In other words, if  $H_+$  differs from  $H_-$ , then the loop has a directionality. If the system is symmetric to inversion we refer to it as *bidirectional* otherwise we refer to it as *directional*. If one of the functions  $H_-$  or  $H_+$  is zero, we refer to the model as *unidirectional*. For examples of directional models see the coupling called ‘telescopic coupling’ by Ottino-Löffler and Strogatz [28], the unidirectional model by Quillen et al. [12] and interactions

with ‘odd coupling’ by Solovov and Friedrich [17].

For a directional model in the form of Eqn. 8 it is convenient to define two functions

$$\begin{aligned} H_s(\psi_1, \psi_2) &\equiv H_+(\psi_1, \psi_2) + H_-(\psi_1, \psi_2) \\ H_a(\psi_1, \psi_2) &\equiv H_+(\psi_1, \psi_2) - H_-(\psi_1, \psi_2). \end{aligned} \quad (9)$$

A bidirectional model (with mirror symmetry) has  $H_a(\psi_1, \psi_2) = 0$ .

### D. Phase differences and the winding number

It is convenient to describe the state of the system with phase shifts or differences between neighboring oscillator phases. We follow Dénes et al. [15] and define the phase difference between two consecutive oscillators with phases  $\theta_i$  and  $\theta_{i-1}$

$$\phi_i \equiv \theta_i - \theta_{i-1} - 2\pi \text{ floor} \left[ \frac{\theta_i - \theta_{i-1} + \pi}{2\pi} \right] \quad (10)$$

where the function  $\text{floor}(x)$  gives the largest integer that is less than  $x$ . The phase difference  $\phi_i \in [-\pi, \pi]$ . To characterize the slope of a state we define a winding number

$$w \equiv \frac{1}{2\pi} \sum_{i=0}^{N-1} \phi_i. \quad (11)$$

It is convenient to compute a quantitive that is proportional to the cumulative sum of the phase differences

$$w_j = \frac{1}{2\pi} \sum_{i=0}^j \phi_i \quad (12)$$

where the winding number  $w = w_{N-1}$ . The periodic boundary condition and Eqn. 10 implies that the sum of the phase differences must be a multiple of  $2\pi$ . This implies that the winding number  $w$  must be an integer, with negative integers or zero allowed [15]. Because the phase shifts are between  $-\pi$  and  $\pi$ , the winding number  $-N/2 \leq w \leq N/2$  with  $w \in \mathbb{Z}$ .

For phase locked or entrained states, phase shifts remain near a particular mean value and the standard deviation of the phase shift remains low. It is convenient to compute the standard deviation of the phase shift

$$\sigma_\phi \equiv \sqrt{\langle (\phi - \bar{\phi})^2 \rangle}. \quad (13)$$

Here the mean phase shift

$$\bar{\phi} = \langle \phi \rangle = \frac{1}{N} \sum_i \phi_i = \frac{2\pi w}{N} \quad (14)$$

is proportional to the winding number  $w$ .

If the system is in a phase locked or entrained state, how is winding number related to the wave speed? The metachronal wave speed  $v_{\text{MW}} \sim \tilde{\omega} dx / \bar{\phi}$  where  $\tilde{\omega} \sim \omega_0$  is the average angular velocity and  $dx$  is the separation between oscillators. This gives  $v_{\text{MW}} \sim \frac{N\tilde{\omega}}{2\pi w} \frac{dx}{N}$ , thus winding number  $w$  and mean phase shift  $\bar{\phi}$  are related to wave travel speed  $v_{\text{MW}}$ .

## II. ASSOCIATED CONTINUUM EQUATIONS

If  $N$  is large and there are no large jumps in phase between neighboring oscillators, the dynamical system of Eqn. 8 can be approximated with a partial differential equation, (e.g., [4, 6]).

We approximate our describe system of oscillators with a continuous function  $\theta(x, t)$  and with coordinate  $x \in [0, 2\pi)$  in an interval. The boundary condition is periodic, so  $\theta(0, t) = \theta(2\pi, t)$ . We associate a position in the interval  $x \in [0, 2\pi)$  for each oscillator in the loop with  $x_j = 2\pi j/N$  giving a separation  $dx = 2\pi/N$  between each oscillator. The continuum variable  $\theta(x, t)$  is related to oscillator phases with  $\theta_j(t) \approx \theta(x_j, t)$  where  $x_j$  are the coordinate positions of each oscillator.

To third order in  $dx$ , where  $dx$  is the separation be-

tween neighboring oscillators

$$\begin{aligned}\theta_{j+1} &\approx \theta_j + dx \frac{\partial \theta}{\partial x} \Big|_{x_j} + \frac{dx^2}{2} \frac{\partial^2 \theta}{\partial x^2} \Big|_{x_j} + \frac{dx^3}{3!} \frac{\partial^3 \theta}{\partial x^3} \Big|_{x_j} \\ \theta_{j-1} &\approx \theta_j - dx \frac{\partial \theta}{\partial x} \Big|_{x_j} + \frac{dx^2}{2} \frac{\partial^2 \theta}{\partial x^2} \Big|_{x_j} - \frac{dx^3}{3!} \frac{\partial^3 \theta}{\partial x^3} \Big|_{x_j}.\end{aligned}\quad (15)$$

We expand the two interaction functions of Eqn. 8, keeping only terms to third order in the phase difference

$$\begin{aligned}H_+(\theta_j, \theta_{j+1}) &= H_+(\psi_1, \psi_2) \Big|_{\psi_1, \psi_2 = \theta_j} \\ &+ \sum_{i=1}^3 \frac{\partial^{(i)} H_+(\psi_1, \psi_2)}{\partial \psi_2^i} \Big|_{\psi_1, \psi_2 = \theta_j} \frac{1}{i!} (\theta_{j+1} - \theta_j)^i.\end{aligned}\quad (16)$$

$$\begin{aligned}H_+(\theta_j, \theta_{j+1}) &= H_+(\psi_1, \psi_2) \Big|_{\psi_1, \psi_2 = \theta_j} \\ &+ \frac{\partial H_+(\psi_1, \psi_2)}{\partial \psi_2} \Big|_{\psi_1, \psi_2 = \theta_j} \left( dx \frac{\partial \theta}{\partial x} + \frac{dx^2}{2} \frac{\partial^2 \theta}{\partial x^2} + \frac{dx^3}{3!} \frac{\partial^3 \theta}{\partial x^3} \right) \\ &+ \frac{\partial^2 H_+(\psi_1, \psi_2)}{\partial \psi_2^2} \Big|_{\psi_1, \psi_2 = \theta_j} \frac{1}{2} \left[ \left( dx \frac{\partial \theta}{\partial x} \right)^2 + dx^3 \frac{\partial \theta}{\partial x} \frac{\partial^2 \theta}{\partial x^2} \right] \\ &+ \frac{\partial^3 H_+(\psi_1, \psi_2)}{\partial \psi_2^3} \Big|_{\psi_1, \psi_2 = \theta_j} \frac{1}{3!} \left( dx \frac{\partial \theta}{\partial x} \right)^3.\end{aligned}\quad (17)$$

In Eqn. 17, the angle  $\theta$  refers to  $\theta(x_j)$  and  $x_j$  is the  $x$ -position of the  $j$ -th oscillator. With the same expansion, we derive similar expressions for  $H_-(\theta_j, \theta_{j-1})$ .

It is convenient to compute derivatives

$$\begin{aligned}c_{0s}(\theta) &= H_s(\theta, \theta) \\ c_{is}(\theta) &= \frac{\partial^{(i)} H_s(\psi_1, \psi_2)}{\partial \psi_2^i} \Big|_{\psi_1, \psi_2 = \theta} \\ c_{ia}(\theta) &= \frac{\partial^{(i)} H_a(\psi_1, \psi_2)}{\partial \psi_2^i} \Big|_{\psi_1, \psi_2 = \theta}.\end{aligned}\quad (18)$$

The index for the coefficient specifies the order of the derivative and the  $a$  or  $s$  specifies which function is used from Eqn. 9.

We insert the expansions of Eqn. 17 and a similar one for  $H_-$  into Eqn. 8 and use short hand  $\theta_{xx} = \frac{\partial^2 \theta}{\partial x^2}$  and  $\theta_t = \dot{\theta}$ , and similarly for other partial derivatives, giving

$$\begin{aligned}\theta_t &= \omega_0 + c_{0s}(\theta) + c_{1a}(\theta) dx \theta_x + c_{1s}(\theta) \frac{dx^2}{2} \theta_{xx} \\ &+ c_{2s}(\theta) \frac{dx^2}{2} (\theta_x)^2 + c_{1a}(\theta) \frac{dx^3}{3!} \theta_{xxx} \\ &+ c_{2a}(\theta) \frac{dx^3}{2} \theta_x \theta_{xx} + c_{3a}(\theta) \frac{dx^3}{3!} (\theta_x)^3.\end{aligned}\quad (19)$$

If the system is bidirectional then the functions  $H_+(\theta) = H_-(\theta)$  and the asymmetric coefficients  $c_{1a} = c_{2a} = c_{3a} =$

0. The partial differential equation in Eqn. 19 becomes (expanding to third order in  $dx$ )

$$\theta_t = \omega_0 + c_{0s}(\theta) + c_{1s}(\theta) \frac{dx^2}{2} \theta_{xx} + c_{2s}(\theta) \frac{dx^2}{2} (\theta_x)^2.\quad (20)$$

Following Pikovsky et al. [4] (their chapter 11), the continuum or large  $N$  limit is taken by multiplying the interaction functions with a strength  $\epsilon$  and then rescaling the strength of the interaction functions in the continuum equation so that they depend on  $dx^2$ . If the interaction functions depend on phase differences, then the coefficients are independent of angle. With a bidirectional equation of motion

$$\frac{d\theta_i}{dt} = \omega_0 + \epsilon [H(\theta_i - \theta_{i+1}) + H(\theta_i - \theta_{i-1})],\quad (21)$$

Eqn. 20 becomes

$$\theta_t = \omega'_0 + \alpha \theta_{xx} + \beta (\theta_x)^2.\quad (22)$$

with  $\tilde{\epsilon} = \epsilon dx^2$  (via the continuum limit) and coefficients  $\alpha = \tilde{\epsilon} H'(0)$ ,  $\beta = \tilde{\epsilon} H''(0)$ , and  $\omega'_0 = \omega_0 + 2H(0)$  [4].

Eqn. 22 is the one dimensional version of Eqn. 11.4 by Pikovsky et al. [4]), has been previously discussed in the context of the non-linear phase equation (Eqn. 10.24 by

[29], and it is related to the Complex Ginzburg Landau equation). With the addition of an additional stochastic term, this equation becomes the Kardar-Parisi-Zhang equation [4, 17] which is used to describe theory of roughening interfaces [30].

Henceforth we don't take the continuum limit, rather we use the associated continuum partial differential equation of Eqn. 19 as an approximation to the more general discrete directional system of Eqn. 8. We discuss each term in the third order (in  $dx$ ) continuum equation of Eqn. 19.

The term with coefficient  $c_{1a}$  is first order in  $dx$  and is  $\propto \theta_x$  so it is an advective term. It is only present if the model is directional. Its coefficient could be dependent upon  $\theta$ . If the time average of  $c_{1a}$  is non-zero then there would be an advection speed associated with perturbations. The term  $\propto \theta_{xx}$  is dispersive and only relevant for directional models.

The term with coefficient  $c_{1s}$  that is  $\propto \theta_{xx}$  is a diffusive term. If this is positive then the system should be stable to small perturbations. Its coefficient could be dependent upon  $\theta$  in which case its time average would be relevant for stability.

The term with coefficient  $c_{2a}$  that is proportional to  $\theta_x \theta_{xx}$  can be considered a diffusive term with sign that depends on the winding number or local slope. This term is only present in directional models. If this term exceeds the term proportional to  $\theta_{xx}$  then only regions where the slope gives a positive term would be stable to growth of small perturbations. If  $c_{2a} > 0$  is positive, then a monotone continuous solution with negative slope  $\theta_x < 0$  could be unstable to growth of small perturbations. The direction of long-lived wave-like states could be set by the sign of this term.

#### A. A condition for stability of a smooth initial condition

Suppose we have a state described with a smooth function  $\theta(x, t)$  at time  $t$  in a directional model. An approximate condition for local stability is that the diffusive terms (those  $\propto \theta_{xx}$ ) in the continuum equation (Eqn. 19) are positive so that short wavelength perturbations are damped diffusively. This implies that a local and slope dependent condition for stability

$$c_{1s}(\theta) + c_{2a}(\theta)dx \theta_x \gtrsim 0. \quad (23)$$

As instability might be slow, the above condition should be satisfied on average, for example averaged over a few oscillation periods if the state is approximately periodic or over a few times the period  $T_0 = 2\pi/\omega_0$ . We denote the averaged coefficients as  $\bar{c}_{1s}$  and  $\bar{c}_{2a}$ . As the condition for instability is dependent upon slope, if there is a sinusoidal perturbation, stability would depend upon the product of its amplitude and wavenumber.

We can relate the stability condition of Eqn. 23 to that of the oscillator chain model by relating the phase shift

$\phi$  between oscillators to the slope;  $\phi \approx \theta_x dx$  where  $dx$  is the separation between oscillators. Eqn. 23 becomes

$$\bar{c}_{1s} + \bar{c}_{2a}\phi \gtrsim 0. \quad (24)$$

In a region where phase shifts between oscillators are similar and equal to  $\phi$ , Eqn. 24 gives a condition on the phase shift for stability.

#### B. The conserved topological charge

If the continuum system has periodic boundary conditions, then the integrated quantity

$$Q = \frac{1}{2\pi} \int_0^{2\pi} dx \theta_x, \quad (25)$$

sometimes called a topological charge, must be equal to an integer [4]. The topological charge  $Q$  measures the phase shift through the loop. This charge is analogous to the winding number  $w$  that we computed for the loop of oscillators (Eqn. 11) and it measures the phase shift across the loop. Furthermore, for the continuum model with a periodic boundary, the topological charge is a conserved quantity. This follows because

$$\dot{Q} = \dot{\theta}(2\pi) - \dot{\theta}(0) = 0. \quad (26)$$

Because of the periodic boundary condition in the equations of motion, the right hand side must vanish.

Conservation of the topological charge  $Q$  in the continuum model (Eqn. 19) implies that initial conditions set the slope of asymptotic solutions [6]. This means that whether an asymptotic state is synchronous or a wave-like state would be determined by initial conditions. A biological system could still tend to form metachronal waves if it does not have periodic boundary conditions. For example, Chakrabarti et al. [6] proposed that gaps in ciliated carpets could facilitate metachronal wave formation. Alternatively, the continuum approximation may fail if discontinuities or short wavelength perturbations are present or develop in the system. The continuum approximation should not hold if there is power at wavevector  $k \sim 1/dx$ . For example, Niedermayer et al. [16] showed that a rotationally symmetric bidirectional model similar to the local Kuramoto model (Eqn. 7) was unstable if the phase differences between oscillators were large, with  $|\phi| > \pi/2$ .

In the subsequent section we investigate the possibility that jumps in phase (discontinuities) between neighboring oscillators in a loop of phase oscillators do not conserve the winding number and so allow wave-like states to develop, independent of the winding number of the initial condition.

### III. NUMERICAL EXPLORATION

We illustrate two models that have been used to describe systems exhibiting metachronal waves, a bidirec-

tional model by Niedermayer et al. [16], and a unidirectional model by Quillen et al. [12]. Numerical integration of the equation, in the form of Eqn. 8 is done with a fixed timestep 4-th order Runge Kutta integrator where each step has duration  $dt$ .

#### A. A bidirectional model by Niedermayer et al. [16]

The model by Niedermayer et al. [16], shown in their Figure 4 and given by their Eqn. 35) with identical intrinsic frequencies and periodic boundary conditions, is described by

$$\frac{d\theta_i}{dt} = \omega_0 + \mu_c (\cos(\theta_i - \theta_{i+1}) + \cos(\theta_i - \theta_{i-1})) - K (\sin(\theta_i - \theta_{i+1}) + \sin(\theta_i - \theta_{i-1})). \quad (27)$$

We relate this model to Eqn. 8 with functions

$$H_+(\psi_1, \psi_2) = H_-(\psi_1, \psi_2) = \mu_c \cos(\psi_1 - \psi_2) - K \sin(\psi_1 - \psi_2). \quad (28)$$

This model is bidirectional as it has  $H_+ = H_-$  and it reduces to the local Kuramoto model of Eqn. 7 with  $\mu_c = 0$ . Computing the coefficients for the continuum model with equations 18

$$\begin{aligned} c_{0s} &= 2\mu_c \\ c_{1a} &= c_{2a} = c_{3a} = 0 \\ c_{1s} &= 2K \\ c_{2s} &= -2\mu_c. \end{aligned} \quad (29)$$

The related continuum model (using Eqn. 19, accurate to third order in  $dx$ ) is

$$\theta_t = \omega_0 + 2\mu_c + K dx^2 \theta_{xx} - \mu_c dx^2 (\theta_x)^2. \quad (30)$$

We note that the continuum model has a diffusive term (that proportional to  $\theta_{xx}$ ) that causes perturbations to diffusively decay when  $K > 0$ . Due to the mirror symmetry (bidirectionality) of the model, the continuum equation lacks a term proportional to  $\theta_x \theta_{xx}$  which could cause a slope dependent instability.

With initial conditions chosen from a uniform distribution (and containing large phase differences) Niedermayer et al. [16] showed that the large phase differences decay, and the system develops a smooth wave-like state. The model is bidirectional so the resulting metachronal waves could be in either direction.

#### B. The unidirectional model by Quillen et al. [12]

We also consider the unidirectional model by Quillen et al. [12] which is

$$\frac{d\theta_j}{dt} = \omega_0 - \frac{\omega_0 K_u}{2} \left[ \tanh \left( \frac{\cos \theta_{j-1} - \cos \theta_j - \beta}{h} \right) + 1 \right]. \quad (31)$$

Here real parameters  $\beta, h > 0$ . The model was motivated by steric interactions between nematodes that reduce the phase velocity for parameter  $K_u > 0$ . In this system, stable long-lived wave-like states are entrained states, as they oscillate in phase velocity [12]. Because the interaction function was motivated by preventing an overlap between neighboring nematode bodies, we sometimes refer to this model as the *overlap* model.

We relate the unidirectional model in Eqn. 31 to Eqn. 8 with functions

$$\begin{aligned} H_+(\psi_1, \psi_2) &= 0 \\ H_-(\psi_1, \psi_2) &= -\frac{\omega_0 K_u}{2} \left[ \tanh \left( \frac{\cos \psi_2 - \cos \psi_1 - \beta}{h} \right) + 1 \right]. \end{aligned} \quad (32)$$

The coefficients for the continuum model, computed using Eqn. 18 are

$$\begin{aligned} c_{0s}(\theta) &= -\frac{\omega_0 K_u}{2} \left[ \tanh \left( \frac{\beta}{h} \right) - 1 \right] \\ c_{1a}(\theta) &= -\frac{\omega_0 K_u}{2} \text{sech}^2 \left( \frac{\beta}{h} \right) \frac{\sin \theta}{h} \\ c_{1s}(\theta) &= -c_{1a}(\theta) \\ c_{2a}(\theta) &= -\omega_0 K_u \text{sech}^2 \left( \frac{\beta}{h} \right) \frac{1}{h^2} \\ &\quad \times \left[ -2 \tanh \left( \frac{\beta}{h} \right) \sin^2 \theta + h \cos \theta \right] \\ c_{2s}(\theta) &= -c_{2a}(\theta) \\ c_{3a}(\theta) &= -\omega_0 K_u \text{sech}^2 \left( \frac{\beta}{h} \right) \frac{\sin \theta}{h} \\ &\quad \times \left[ 2 \tanh^2 \left( \frac{\beta}{h} \right) \frac{\sin^2 \theta}{h^2} - \text{sech}^2 \left( \frac{\beta}{h} \right) \frac{\sin^2 \theta}{h^2} \right. \\ &\quad \left. - 2 \tanh \left( \frac{\beta}{h} \right) \frac{\cos \theta}{h} - \frac{1}{2} \right]. \end{aligned} \quad (33)$$

If  $K_u$  is not large then we can assume that the oscillator phases advance at a nearly constant rate. We can approximately average over an oscillation cycle by integrating over  $\theta$ . We define an averaged coefficient with

$$\bar{c} \approx \frac{1}{2\pi} \int_0^{2\pi} d\theta c(\theta). \quad (34)$$

Taking the averages of the coefficients of Eqn. 33,

$$\begin{aligned} \bar{c}_{1s} &= \bar{c}_{1a} = c_{3a} = 0 \\ \bar{c}_{2a} &= -\bar{c}_{2s} = \frac{\omega_0 K_u}{h^2} \text{sech}^2 \left( \frac{\beta}{h} \right) \tanh \left( \frac{\beta}{h} \right). \end{aligned} \quad (35)$$

Because the coefficient  $c_{0s}(\theta)$  is independent of  $\theta$ , the average  $\bar{c}_{0s} = c_{0s}$ .

Using the averaged coefficients in equations 35, the continuum equation (Eqn. 19) for the unidirectional

TABLE I. Integration parameters for unidirectional and bidirectional models

Unidirectional model (Eqn. 31, continuum equation Eqn. 36)						
Common parameters	$K_u$	$\beta$	$h$	$N$	$dt$	$t_{\max}$
	0.7	0.1	0.05	200	0.05	600
Integration names	Uni-S1	Uni-S4	Uni-U			
Initial condition	sine	sine	uniform			
Amplitude $A_{\text{init}}$	0.5	0.02	-			
Wavelength $n_\lambda$	1	4	-			
Figures	1, 2a	2b	3a			
Bidirectional model (Eqn. 27, continuum equation Eqn. 30)						
Common Parameters	$K$	$\mu_c$	$N$	$dt$	$t_{\max}$	
	0.03	0.05	100	0.05	300	
Integration name	Bi-U					
Initial condition	uniform					
Figure	3b					

Notes:  $n_\lambda$  is the number of wavelengths that fit within the loop of oscillators for the sinusoidal initial condition. When initial conditions are uniform, the initial phases for each oscillator are independently drawn from a uniform distribution within  $[0, 2\pi)$ . All models have intrinsic angular frequency  $\omega_0 = 1$  and a periodic boundary condition.

model of Eqn. 31 becomes

$$\theta_t = \omega_0 - \frac{\omega_0 K_u}{2} \left[ \tanh\left(\frac{\beta}{h}\right) - 1 \right] + \omega_0 K_u \text{sech}^2\left(\frac{\beta}{h}\right) \tanh\left(\frac{\beta}{h}\right) \frac{dx^2}{2h^2} [-(\theta_x)^2 + dx \theta_x \theta_{xx}]. \quad (36)$$

As the continuum equation lacks a second order term proportional to  $\theta_{xx}$ , equations 23 would be violated for negative slopes (assuming  $K_u > 0$ ). Thus instability caused by the  $\theta_x \theta_{xx}$  term is expected where the slope or phase shifts are locally negative, even when the magnitude of the phase shift is small. This suggests that the synchronous state itself is unstable. By linearizing about the synchronous state and averaging over time, it is possible to show that this is true, though the associated Jacobian matrix is degenerate.

### C. Illustrations of numerical integrations

Parameters for unidirectional and bidirectional model integrations are listed in Table I. We group integrations by the dynamical system integrated, and refer to the equation describing it in the table. The number of oscillators in the loop is  $N$  and  $dt$  is the time-step used for each single 4-th order Runge Kutta integration step. All models have intrinsic frequency  $\omega_0 = 1$ . Total integration time is  $t_{\max}$ .

The initial conditions for the unidirectional integra-

tions, denoted Uni-S1 and Uni-S4, are a sine

$$\theta_j(t=0) = A_{\text{init}} \sin(2\pi n_\lambda j/N) \quad (37)$$

with amplitude  $A_{\text{init}}$  and integer  $n_\lambda$  that determines how many wavelengths fit within the loop. For the Uni-U and Bi-U integrations, initial phases are independently drawn from a uniform probability distribution  $\in [0, 2\pi)$ .

In Figure 1 we show the Uni-S1 integration of the unidirectional model with an initial sine perturbation. In this figure integration time is along the  $x$  axis. For the top three panels, the  $y$  axis is the index of the oscillator  $j$ . In the top three panels we show phase  $\theta_j$ , phase difference  $\phi_j$  (as defined in Eqn. 10), and the cumulative sum  $w_j$  of the phase differences, as defined in Eqn. 12. The bottom panel plots the winding number  $w$  (defined in Eqn. 11 and equal to  $w_{N-1}$ ). The cumulative sum of the phase difference shows where differences in the winding number arise. The integration shows that a smooth initially smooth state develops regions where there are jumps in phase between neighboring oscillators. We can think of them as discontinuities but they consist of pairs or groups of oscillators with phase shifts that alternate by approximately  $\pi$ . The changes in the winding number occur where phase differences are near  $\pi$ . When two consecutive oscillators have a phase difference of  $\pi$ , a small change in the phase difference can cause a change of  $\pm 1$  in the winding number. At the end of the integration the winding number is 9 and a metachronal wave has emerged, even though the initial condition had a winding number of zero.

In Figure 2 we show phases as a function of oscillator index at different times in two integrations of the unidirectional model of Eqn. 31, the Uni-S1 and Uni-S4 integrations. The Uni-S4 integration also has a small sinusoidal initial perturbation but it is shorter wavelength and lower amplitude than that in the Uni-S1 integration. Figure 2 shows that the short wavelength perturbations only grow where the phase difference (or slope) is negative. The continuum approximation for this model (Eqn. 36) contains a term proportional to  $\theta_x \theta_{xx}$  which causes instability depending upon the sign of the slope. For  $K_u > 0$  the sign of this term is only positive if  $\theta_x > 0$ . This means that instability is expected if the slope or phase difference is negative. This expectation is consistent with what is seen in Figure 2. The times of the plotted curves are  $t = 1, 20, 50, 91, 106, 108$  in Figure 2a and  $t = 1, 100, 200, 300, 330, 340, 350$  in Figure 2b.

The bidirectional model (Eqn. 27) exhibits some differences when compared to the unidirectional model. For the bidirectional model, when the initial conditions are smooth, and phase differences between neighboring oscillators are small, the winding number is conserved. This is consistent with the stability limit computed by Niedermayer et al. [16] who found that instability arises only if phase differences exceed  $\pm\pi/2$ . In the unidirectional model, even smooth initial conditions can lead to growth of large phase differences (depending upon the sign of the slope).

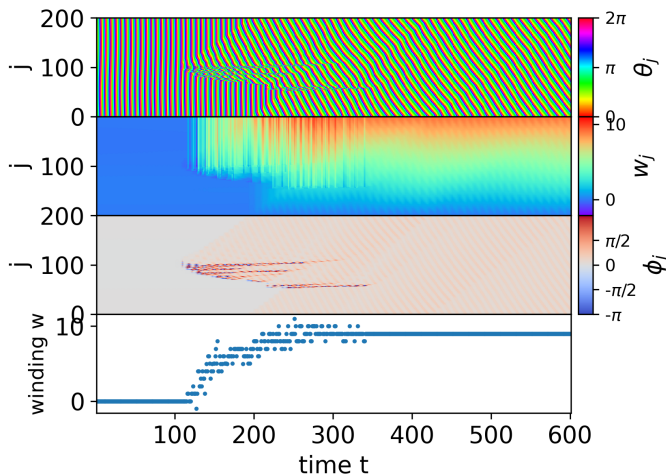


FIG. 1. An integration, labelled Uni-S1 of the unidirectional model given in Eqn. 31. The parameters for the model are listed in Table I. The initial condition is a sine wave and the boundary condition is periodic. The top panel shows phase  $\theta_j$  for each oscillator as a function of index  $j$ , where index  $j$  increases on the  $y$  axis and as a function of time which increases on the  $x$  axis. The second panel from top shows the cumulative sum  $w_j$  of phase differences (defined in Eqn. 12). The phase differences  $\phi_j$  (defined in Eqn. 10) are shown in the third panel. The winding number  $w = w_{N-1}$  (defined in Eqn. 11) is computed from the sum of the phase differences and is shown in the bottom panel. Groups of oscillators that have phases that differ by about  $\pi$  develop, and cause jumps in the cumulative sum of phase differences and these give changes in the winding number  $w$ . At the end of the integration, variations in winding number cease and a wave-like state is maintained.

If initial conditions contain large jumps in phase, then discontinuities can persist that cause variations in winding number in both bidirectional and unidirectional models. We show two integrations, one for the unidirectional model (denoted Uni-U) and one for the bidirectional model (denoted Bi-U). The phases for these integrations are independently initialized with random angles drawn from uniform probability distributions in  $[0, 2\pi)$ . These integrations are shown in Figure 3 and the parameters of the models are listed in Table I. In both models, jumps in phase cause changes in winding number. However, over long periods of time the high frequency power decays and both system approach a long lived solution with an approximately constant slope. After the decay of the large jumps in phase, variations in winding number cease.

In the unidirectional model, both continuous and random initial conditions generate a wave-like state with a preferred direction. However, in the bidirectional model, only initial conditions that include jumps in phase allow variations in winding number. In the unidirectional model, jumps in phase resolve into waves traveling in a single direction, whereas in the bidirectional model jumps in phase resolve into clusters of oscillators exhibiting

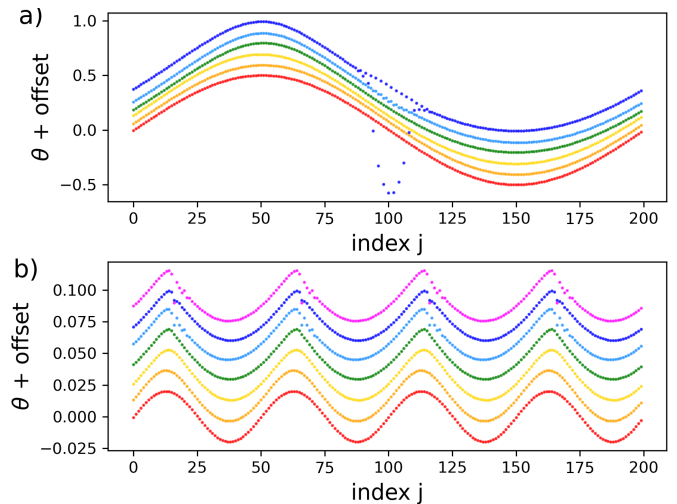


FIG. 2. Evolution of the unidirectional model (Eqn. 31) with initial sinusoidal perturbations. a) We show the Uni-S1 integration with an initial sine perturbation with wavelength that exactly fits within the loop. b) We show the Uni-S4 integration where the initial sine perturbation is small and has wavelength  $1/4$  of the length of the loop. The phases  $\theta_j$  of each oscillator are plotted at different times as a function of index  $j$  (on the  $x$  axis) labeling the oscillator. The oscillator phases at the different times have been offset so that the curves are plotted in order of time, with the later times on the top. While the initial conditions (shown red as the bottom curves) are smooth, non-linearity in the model causes an increase in the height of the peaks. Regions with negative phase difference (negative slope) are unstable to the growth of short wavelength perturbations.

waves that travel in either direction. In the bidirectional model, and with smooth initial conditions, the direction of an emergent wave is set by the initial winding number. Because regions of negative slope can result in instability in the unidirectional model, a smooth initial condition with an initial winding number of zero can still lead to an emergent wave. With random initial conditions, emergent waves in either direction are equally likely for the bidirectional model. In the unidirectional model, emergent waves only travel in one direction. In both models, there are multiple stable long live entrained states, that are characterized by different winding numbers.

#### D. Causing instability in a bidirectional model to make an adjustable directional model

To explore how directionality affects the behavior of oscillator chain models, we desire simple models with sufficient numbers of parameters that we can smoothly adjust whether it is directional or bidirectional. We modify the sinusoidal bidirectional model in section III A, Eqn. 27,



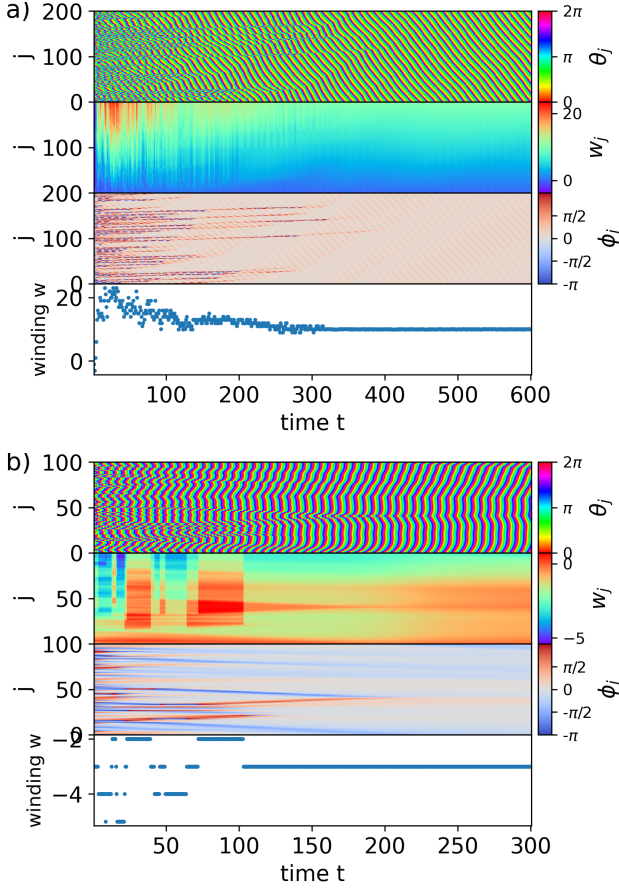


FIG. 3. Similar to Figure 1 except the initial conditions are drawn from a uniform distribution  $\in [0, 2\pi)$ . a) We show the unidirectional Uni-U integration. b) We show the bidirectional Bi-U integration. Groups of oscillators that have phase differences of about  $\pi$  cause jumps in the cumulative sum of phase differences. The initial conditions have large phase differences, and while these persist, the winding number is not conserved. Clusters of oscillators form in wave-states with waves going in either direction in the bidirectional model but only moving in a single direction in the unidirectional model. After large phase differences decay, the winding number ceases to vary in both models.

so that it can be directional

$$\frac{d\theta_i}{dt} = \omega_0 + \mu_{c+} \cos(\theta_i - \theta_{i+1}) + \mu_{c-} \cos(\theta_i - \theta_{i-1}) - K_+ \sin(\theta_i - \theta_{i+1}) - K_- \sin(\theta_i - \theta_{i-1}). \quad (38)$$

With  $K_+ = K_-$  and  $\mu_{c+} = \mu_{c-}$  we recover the bidirectional model of Eqn. 27. The interaction functions are

$$\begin{aligned} H_+(\theta_i, \theta_{i+1}) &= \mu_{c+} \cos(\theta_i - \theta_{i+1}) - K_+ \sin(\theta_i - \theta_{i+1}) \\ H_-(\theta_i, \theta_{i-1}) &= \mu_{c-} \cos(\theta_i - \theta_{i-1}) - K_- \sin(\theta_i - \theta_{i-1}). \end{aligned} \quad (39)$$

TABLE II. Integration parameters for directional models

Directional sinusoidal model (Eqn. 38)						
Associated continuum equation (Eqn. 41)						
Common Parameters	$K_+$	$K_-$	$\mu_{c+}$	$N$	$dt$	$t_{\max}$
	0.01	0.01	0	64	0.05	450
Integration series name	Di-Series-A					
Type of initial condition	sine, $n_\lambda = 4$					
Amplitude $A_{\text{init}}$	[0,0.5]					
Parameter $\mu_{c-}$	[0,0.9]					
Figure	4					
Directional overlap model (Eqn. 45)						
Associated continuum equation (Eqn. 46)						
Common Parameters	$\beta$	$h$	$K$	$N$	$dt$	$t_{\max}$
	0.1	0.05	0.01	64	0.05	600
Integration series name	Di-Series-B					
Type of initial condition	sine, $n_\lambda = 4$					
Amplitude $A_{\text{init}}$	[0.01,0.4]					
Parameter $K_u$	[0.01,0.4]					
Figure	5					

Notes: All models have intrinsic angular frequency  $\omega_0 = 1$  and a periodic boundary condition. For integration series we show ranges for varied parameters.

The coefficients computed via Eqn. 18 become

$$\begin{aligned} c_{0s} &= \mu_{c+} + \mu_{c-} \\ c_{1a} &= K_+ - K_- \\ c_{1s} &= K_+ + K_- \\ c_{2a} &= -\mu_{c+} + \mu_{c-} \\ c_{2s} &= -c_{0s} \\ c_{3a} &= -c_{1a}, \end{aligned} \quad (40)$$

and are independent of  $\theta$ .

The related continuum model (using Eqn. 19, accurate to third order in  $dx$ ) is

$$\begin{aligned} \theta_t &= \omega_0 + \mu_{c+} + \mu_{c-} + (K_+ + K_-) \frac{dx^2}{2} \theta_{xx} \\ &\quad - (\mu_{c+} + \mu_{c-}) \frac{dx^2}{2} (\theta_x)^2 + (K_+ - K_-) \frac{dx^2}{2} \theta_{xxx} \\ &\quad + (-\mu_{c+} + \mu_{c-}) \frac{dx^3}{2} \theta_x \theta_{xx} + (K_+ - K_-) \frac{dx^3}{3!} (\theta_x)^3. \end{aligned} \quad (41)$$

For instability caused by the  $\theta_x \theta_{xx}$  term that is sensitive to the sign of the slope, Eqn. 23 approximately gives

$$(\mu_{c+} - \mu_{c-})(dx \theta_x) \gtrsim (K_+ + K_-). \quad (42)$$

For phase shift  $\phi$  between oscillators, this condition for instability (following Eqn. 24) becomes

$$(\mu_{c+} - \mu_{c-})\phi \gtrsim (K_+ + K_-). \quad (43)$$

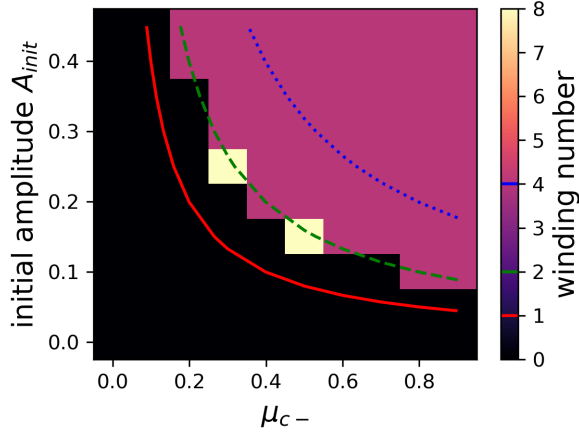


FIG. 4. We integrate the directional sinusoidal model of Eqn. 38 with a sinusoidal initial condition with a range of initial amplitudes  $A_{\text{init}}$ , on the  $y$  axis, and a range for the parameter  $\mu_{c-}$ , on the  $x$  axis. Remaining parameters for the series of integrations are listed in Table II with the name Di-Series-A. The initial winding number  $w = 0$ . Plotted as an image is the final winding number at the end of each integration. A change in winding number implies that an instability occurred during the integration. The contours show the stability parameter  $y_{\text{crit}}$  of Eqn. 44 which is derived by comparing the strength of diffusive terms in the continuum equation (following Eqn. 43). We plot  $y_{\text{crit}} = 1$  (red solid line), 2 (green dashed line) and 4 (blue dotted line). When the stability parameter  $y_{\text{crit}}$  is greater than 1, and to the right of the red solid line, instability occurs giving clusters of oscillators with larger phase differences. These resolve by increasing the winding number.

The sign of  $\mu_{c+} - \mu_{c-}$  determines the sign of unstable slopes.

To check to see if we can predict when a system develops instability we run a series of integrations, denoted Di-Series-A in Table II, that begin with a small sinusoidal variation and a winding number of zero. We measure the change in winding number after integrating a specific period of time. The model has common parameters  $N = 64$ ,  $K_+ = K_- = 0.01$ ,  $\omega_0 = 1$ , and  $\mu_{c+} = 0$ . The sinusoidal initial condition has  $n_\lambda = 4$  wavelengths within the loop of oscillators. We do integrations with a range of amplitudes  $A_{\text{init}}$  for the initial condition and a range of parameter  $\mu_{c-}$ . In each integration, we measure the winding number at the end of the integration. The final winding number is plotted as an image in Figure 4. Integrations in which perturbations grow exhibit changes in winding number.

For the integrations shown in Figure 4, the maximum phase shift in the initial condition depends on the amplitude and wavelength of the sine  $|\phi_{\text{max}}| = A_{\text{init}} n_\lambda dx$  with

$dx = 2\pi/N$ . The contours in Figure 4 show the value of

$$\begin{aligned} y_{\text{crit}}(A_{\text{init}}, \mu_{c-}) &= |\phi_{\text{max}}| \frac{|\mu_{c+} - \mu_{c-}|}{(K_+ + K_-)} \\ &= A_{\text{init}} n_\lambda \frac{2\pi}{N} \frac{|\mu_{c+} - \mu_{c-}|}{(K_+ + K_-)}, \end{aligned} \quad (44)$$

which is derived from the stability limit estimate of Eqn. 43. Near where this function is above 1, we expect instability. This is indeed seen in these numerical integrations as changes in winding number are only seen to the right of the solid red contour which has  $y_{\text{crit}} = 1$ . We numerically confirm that Eqn. 24 can give a slope dependent estimate for the local stability of smooth initial conditions in a directional model.

### E. Stabilizing a unidirectional model to make an adjustable directional model

The unidirectional model discussed in section III B (Eqn. 31), when averaged has coefficient  $\bar{c}_{1s} = 0$ , so its associated continuum equation (Eqn. 36) lacks a stabilizing term proportional to  $\theta_{xx}$ . To this unidirectional model, we add an additional term, that with coefficient  $K$  from the bidirectional model of Eqn. 27, that gives a non-zero coefficient  $c_{1s}$  (see section III A);

$$\begin{aligned} \frac{d\theta_j}{dt} &= \omega_0 - \frac{\omega_0 K_u}{2} \left[ \tanh \left( \frac{\cos \theta_{j-1} - \cos \theta_j - \beta}{h} \right) + 1 \right] \\ &\quad - K [\sin(\theta_j - \theta_{j+1}) + \sin(\theta_j - \theta_{j-1})]. \end{aligned} \quad (45)$$

With the addition of the term with coefficient  $K$ , the model is no longer unidirectional, rather it is directional and we can adjust the relative strengths of the symmetric and antisymmetric interactions by varying  $K$ .

The averaged coefficients present in the continuum equation for this model are the same as in equations 35, except the coefficient  $c_{1s} = 2K$ . The associated continuum equation is similar to Eqn. 36 but with an additional term,

$$\begin{aligned} \theta_t &= \omega_0 - \frac{\omega_0 K_u}{2} \left[ \tanh \left( \frac{\beta}{h} \right) - 1 \right] + K dx^2 \theta_{xx} \\ &\quad + \omega_0 K_u \text{sech}^2 \left( \frac{\beta}{h} \right) \tanh \left( \frac{\beta}{h} \right) \frac{dx^2}{2h^2} [-(\theta_x)^2 + dx \theta_x \theta_{xx}]. \end{aligned} \quad (46)$$

As in section III D, we run a series of integrations, denoted Di-Series-B and with parameters listed in Table II, have sinusoidal initial conditions, and cover a range of amplitudes and parameters  $K_u$  to see which ones develop instabilities that cause variations in winding number. The final winding numbers are plotted in figure 5. These integrations have parameters  $h, \beta, \omega_0$  giving coefficient  $\bar{c}_{2a} \approx 27K_u$  (evaluated using Eqn. 35). The coefficient  $c_{1s} = 2K$  for this dynamical system. The estimate

for instability of Eqn. 24 depends on

$$y_{\text{crit}}(A_{\text{init}}, K_u) \approx 13A_{\text{init}}n_\lambda \frac{2\pi}{N} \frac{K_u}{K}, \quad (47)$$

with unstable phase shifts for a sinusoidal initial condition likely for  $y_{\text{crit}} \gtrsim 1$ . Contours with  $y_{\text{crit}} = 1, 2, 4$  are shown on Figure 5. The  $y_{\text{crit}} = 1$  curve delineates the region where winding number remains fixed. Thus Figure 5 illustrates that the condition (Eqn. 24) based on coefficients of diffusive terms in the associated continuum equation is consistent with the development of short wavelength instabilities in the dynamical system of Eqn. 45.

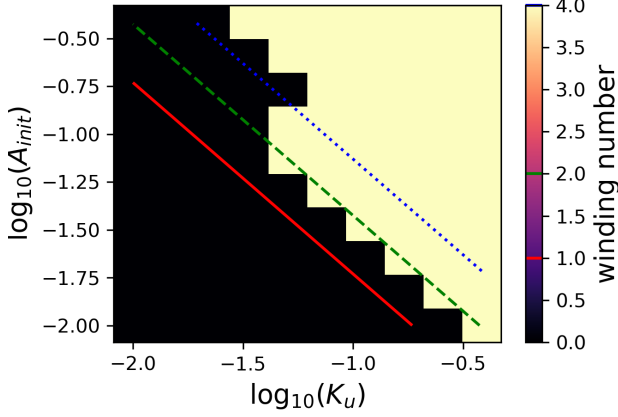


FIG. 5. Similar to Figure 4 except we integrate the directional overlap model of Eqn. 45 with a sinusoidal initial condition. Integrations have a range of initial amplitudes  $A_{\text{init}}$ , shown with a log-scale on the  $y$  axis, and a range for the parameter  $K_u$ , shown with a log-scale on the  $x$  axis. Remaining parameters for the series of integrations are listed in Table II with the name Di-Series-B. Plotted as an image is the final winding number at the end of each integration. A change in winding number implies that an instability occurred during the integration. The contours show the stability parameter  $y_{\text{crit}}$  of Eqn. 47, which is derived by comparing the strength of diffusive terms in the continuum equation. We plot  $y_{\text{crit}} = 1$  (red solid line), 2 (green dashed line) and 4 (blue dotted line). When the stability parameter  $y_{\text{crit}}$  is greater than 1, and to the right of the red solid line, instability occurs giving perturbations in regions where the slope (or equivalently the phase difference) is negative. These resolve by increasing the winding number.

#### IV. STOCHASTIC DIRECTIONAL PHASE OSCILLATOR MODELS

In the previous sections we found that the initial condition can affect the properties of the system after integration. How is it possible for a biological system to ensure that a metachronal wave is robustly generated? As fluctuations are likely to be present in ciliated systems (e.g., [19]) and following Solovev and Friedrich [17], we consider the role of white noise in influencing the properties of long-lived states.

To the each oscillator in the direction models of Eqns. 38 and 45 we add a continuous random variable that is Gaussian white noise,  $\xi(t)$ . We characterize the strength of the noise with parameter  $\eta$  where the probability distribution of the integral  $W(\Delta t) = \int_0^{\Delta t} \xi(t)dt$  is a normal distribution with zero mean and with variance  $\eta\Delta t$ . Equivalently  $\langle \xi(t)\xi(t') \rangle = \eta\delta(t-t')$ . In our numerical integrations, at each time step of duration  $dt$  we add an independent random variable to each oscillator phase that is drawn from a normal distribution with zero mean and variance  $\eta dt$ .

##### A. A sinusoidal directional model with white noise

We modify the directional model of Eqn. 38 discussed in section III D with the addition of a stochastic term

$$\begin{aligned} \frac{d\theta_i}{dt} = & \omega_0 + \mu_{c+} \cos(\theta_i - \theta_{i+1}) + \mu_{c-} \cos(\theta_i - \theta_{i-1}) \\ & - K_+ \sin(\theta_i - \theta_{i+1}) - K_- \sin(\theta_i - \theta_{i-1}) \\ & + \xi_i(t). \end{aligned} \quad (48)$$

Here each  $\xi_i(t)$  is an independent continuous random variable that is Gaussian white noise with strength  $\eta$ , as discussed at the beginning of section IV.

The associated continuum equation for the model of Eqn. 48 is the same as Eqn. 41 with the addition of white noise that depends on both space and time;

$$\begin{aligned} \theta_t = & \omega_0 + \mu_{c+} + \mu_{c-} + (K_+ + K_-) \frac{dx^2}{2} \theta_{xx} \\ & - (\mu_{c+} + \mu_{c-}) \frac{dx^2}{2} (\theta_x)^2 + (K_+ - K_-) \frac{dx^2}{2} \theta_{xxx} \\ & + (-\mu_{c+} + \mu_{c-}) \frac{dx^3}{2} \theta_x \theta_{xx} + (K_+ - K_-) \frac{dx^3}{3!} (\theta_x)^3 \\ & + \xi(x, t). \end{aligned} \quad (49)$$

Here  $\xi(x, t)$  denotes uncorrelated Gaussian white noise with  $\langle \xi(x, t)\xi(x', t') \rangle = D\delta(x-x')\delta(t-t')$ . We relate  $D$  to the noise strength  $\eta$  for the discrete system via  $D = \eta dx$  where  $dx$  is the distance between neighboring oscillators.

We run a series of integrations of Eqn. 48, where initial phases are all set to zero, so the system begins in the synchronous state. In these models we set  $K_+ = K_-$  and  $\mu_{c+} = 0$ . We vary the strength of the noise  $\eta$  and the parameter  $\mu_{c-}$  which makes the model directional. The integrations denoted DWN1 and DWN2, have parameters listed in Table III and are shown in Figure 6. In both integrations the noise seeds perturbations that grow sufficiently large that they cause variations in winding number. As the phase jumps resolve, the system enters a coherent wave state that persists.

The DWN1 integration, shown in Figure 6a has parameter  $\mu_{c-}$  with opposite sign to that of the DWN2 model, which is shown in Figure 6b. The sign difference causes the resultant waves to be in opposite directions. The DWN2 integration has stronger noise than

TABLE III. Parameters for integrations of directional models with noise

Directional sinusoidal model with white noise (Eqn. 48)						
Associated stochastic continuum equation (Eqn. 49)						
Common parameters	$K_+$	$K_-$	$\mu_{c+}$	$dt$	$t_{\max}$	
	0.01	0.01	0	0.05	600	
Integrations	DWN1	DWN2	DWN-SerA	DWN-SerW	DWN-SerN	BWN-SerN
Noise strength $\eta$	0.005	0.02	[ $10^{-3}$ ,0.09]	[ $10^{-3}$ ,0.04]	[ $10^{-3}$ ,0.03]	[ $10^{-3}$ ,0.03]
Parameter $\mu_{c-}$	-0.006	0.03	[-0.07,0.07]	0.06	0.06	0.0
Initial winding number $w_0$	0	0	0	[-15,15]	0	0
Number of oscillators $N$	50	50	50	50	[32,4096]	[32,4096]
Figures	6a	6b	7	9a,b	10a,b	10e,f
Directional overlap model with white noise (Eqn. 50)						
Associated stochastic continuum equation (Eqn. 51)						
Common parameters	$\beta$	$h$	$dt$	$t_{\max}$		
	0.1	0.05	0.05	600		
Integrations	OWN-SerA	OWN-SerB	OWN-SerC	OWN-SerW	OWN-SerN	
Noise strength $\eta$	$10^{-3}$	[ $10^{-4}$ ,0.04]	[ $10^{-4}$ ,0.04]	[ $10^{-3}$ ,0.04]	[ $10^{-3}$ ,0.03]	
Parameter $K$	[0.0003,0.13]	0.002	[0.0006,0.26]	0.01	0.01	
Parameter $K_u$	[0.01,0.41]	[0.01,0.28]	0.2	0.2	0.2	
Initial winding number $w_0$	0	0	0	[-15,15]	0	
Number of oscillators $N$	100	100	100	50	[32,4096]	
Figures	8a,b	8c,d	8e,f	9c,d	10c,d	

Notes: All models have intrinsic angular frequency  $\omega_0 = 1$  and a periodic boundary condition. Initial conditions have a constant slope. The initial phase differences are determined by the initial winding number  $w_0$ . For integration series we show ranges for the varied parameters.

the DWN1 integration. While the winding number remains constant at the end of the DWN1 integration, it continues to vary in the DWN2 integration. The phase shift is fairly smooth in the DWN1 integration, indicating that the phase shift is sufficiently high that perturbations caused by the noise are damped diffusively. We attribute the increased stability to the strength of the slope dependent diffusion term, proportional to  $\theta_x \theta_{xx}$ , in the associated continuum equation, is Eqn. 49.

The higher level of noise in the DWN2 integration, shown in Figure 6b, causes changes in the winding number to persist throughout the integration. While the winding number never drops to zero, variations in slope or phase shift persist and only clusters of oscillators maintain a constant phase delay. This integration has a higher value of the standard deviation of the phase shift than the DWN1 integration, indicating that the wave is not entirely coherent. There are regions or clusters of oscillators in wave-like states with jumps in phase between them. The sensitivity of the collective motion to the strength of the noise is consistent with the study by Solovov and Friedrich [17] who found that white noise could suppress synchronization in two-dimensional models of interacting phase oscillators.

We run a series of integrations varying the strength of the noise  $\eta$  and the  $\mu_{c-}$  parameter setting the asymmetry in the interactions. The series is denoted DWN-SerA in Table III. At the end of each integration we record

the winding number  $w$  and the standard deviation of the phase difference  $\sigma_\phi$ . Both quantities are plotted as images in Figure 7. We use  $\sigma_\phi$  to characterize the coherence of wave-like states at the end of the integrations.

Figure 7a shows that wave-like states are long lived in the presence of noise and it is possible to chose the direction of the waves by adjusting the sign of the parameter  $\mu_{c-}$ . In these integrations  $\mu_{c+} = 0$ . More generally the sign of  $\mu_{c+} - \mu_{c-}$  would determine the direction of the waves. This follows as this difference sets the sign of the  $c_{2a}$  coefficient which in turn determines the sign of the  $\theta_x \theta_{xx}$  term in the associated continuum equation (Eqn. 41).

The size of term that is proportional to  $\theta_{xx}$  in the continuum equation (Eqn. 41) depends on  $c_{1s} = (K_+ + K_-)$  (Eqn. 40). As the coefficient is positive, this diffusive term damps short wavelength perturbations. The linearized stochastic continuum equation would resemble the Edwards-Wilkinson equation, where the variance of the phase is sensitive to the ratio  $\eta/(K_+ + K_-)$ , which is why we use  $\eta/(K_+ + K_-)$  on the  $y$  axis in Figure 7.

Slope dependent instability depends on the size of the term that is proportional to  $\theta_x \theta_{xx}$  in the continuum equation (Eqn. 49). This term depends on the coefficient  $c_{2a} = -\mu_{c+} + \mu_{c-}$  (Eqn. 40). The slope dependent stability condition depends on the ratio of  $c_{2a}$  and  $c_{1s} = K_+ + K_-$  (Eqn. 23) which is why we use  $\mu_{c-}/(K_+ + K_-)$  on the  $x$  axis. With noise able to

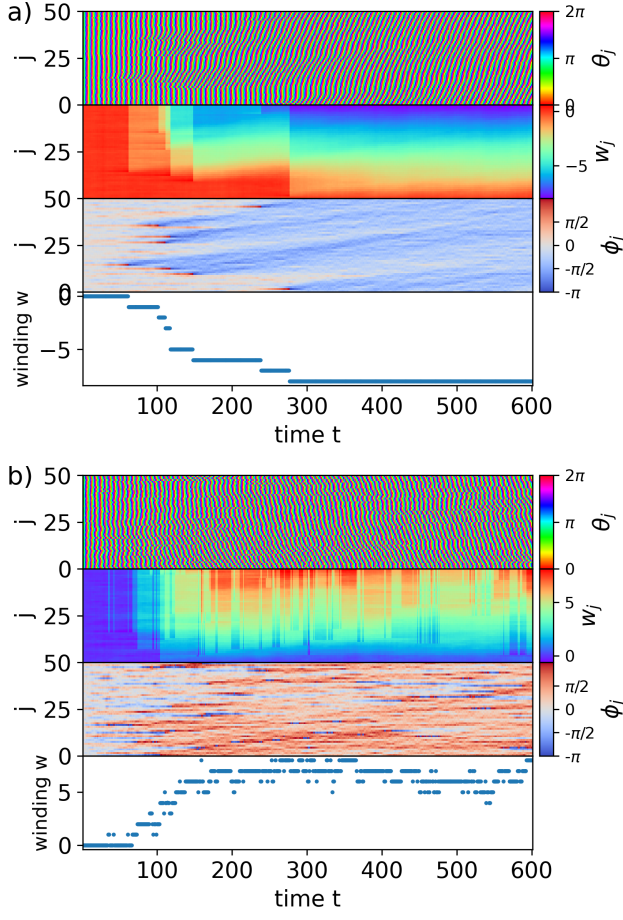


FIG. 6. Similar to Figure 1 except we show two integrations of the stochastic directional sinusoidal model of Eqn. 48, with parameters listed in Table III. Initially all oscillator phases are set to zero. a) We show the DWN1 integration. This model has enough noise to seed perturbations that grow. Groups of oscillators that have phase differences of about  $\pi$  cause jumps in the cumulative sum of phase differences, and these cause variations in the winding number. These groups resolve into negative phase differences and the system enters a long-lived wave-like state. We attribute the later stability of the resulting wave to the slope dependent diffusive term in the continuum equation (that  $\propto \theta_x \theta_{xx}$ ). b) We show the DWN2 integration. This model has  $\mu_{c-}$  with the opposite sign as the DWN1 model, so noise induced perturbations resolve into a wave that travels in the opposite direction. The noise strength is higher in this integration so only clusters of oscillators maintain a constant phase delay and the winding number continues to vary.

cause jumps in phase ( $\eta/(K_+ + K_-)$  not too small) and jumps in phase able to cause changes in winding number  $|\mu_{c-}|/(K_+ + K_-) \gtrsim 1$ , the system maintains a wave-like state. With larger  $\eta/(K_+ + K_-)$  the noise dominates over local synchronization causing the system to lose coherence. The system breaks up into clusters of oscillators that are moving together. This is evident in Figure 7b showing the standard deviation of the phase shift  $\sigma_\phi$

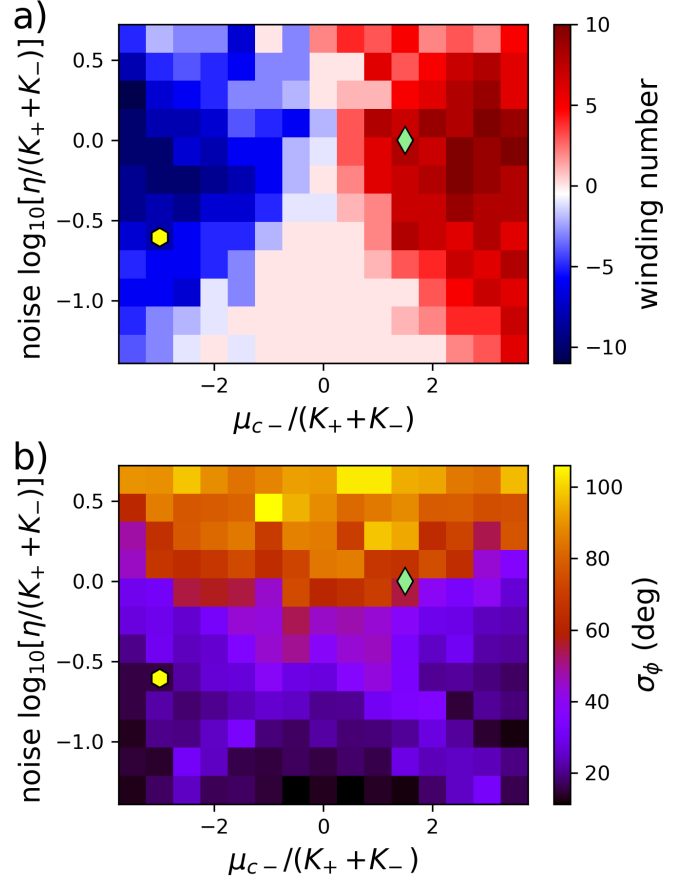


FIG. 7. We show integration series denoted DWN-SerA with different levels of white noise strength  $\eta$  and parameter  $\mu_{c-}$  for the directional sinusoidal model of Eqn. 48. Parameters for the integrations are given in Table III. a) We show final winding number as an image. b) We show the standard deviation of the average phase difference  $\sigma_\phi$  (defined in Eqn. 13). The blue diamond shows the DWN1 integration of Figure 6a and the yellow hexagon shows the DWN2 integration of Figure 6b. The direction of the waves is set by the parameter  $\mu_{c-}$ . Simulations with sufficient noise and asymmetry in nearest neighbor interaction functions enter wave-like states, but if the noise is too strong, coherence is reduced or lost.

(computed with Eqn. 13). When the wave is coherent across the system, the standard deviation  $\sigma_\phi$  is lower ( $\lesssim 20^\circ$ ). When the system loses coherence and breaks up into small clusters,  $\sigma_\phi$  is higher.

Two integrations with the same value of  $\eta$  and  $\mu_{c-}$  can give different final winding numbers, but the scatter in final winding numbers is not large. This can be seen from the differences in final winding between neighboring pixels in Figure 7a, as each pixel represents a single numerical integration.



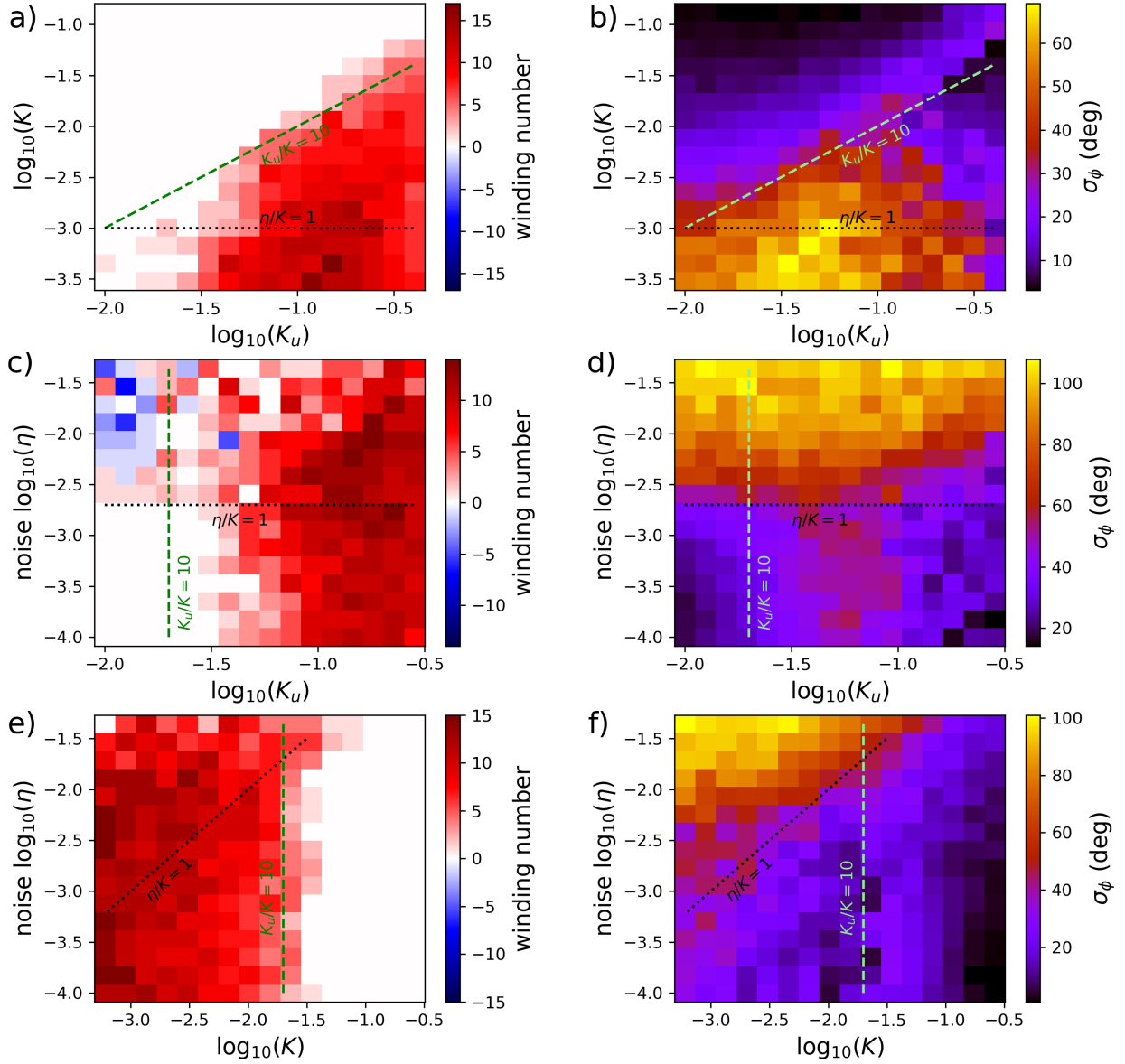


FIG. 8. a) We show final winding number as a image for the OWN-SerA integrations with different parameters  $K$  and  $K_u$  for the model of Eqn. 50. b) Similar to a) except we show the final value of the standard deviation of the phase shift  $\sigma_\phi$  for the OWN-SerA integrations. c) Similar to b) but showing the winding number for the OWN-SerB integrations with different noise strength  $\eta$  and parameter  $K_u$ . d) Similar to c) but showing the final value of the standard deviation of the phase shift  $\sigma_\phi$  for the OWN-SerB integrations. e) Similar to a) except we show the final value of the standard deviation of the phase shift  $\sigma_\phi$  for the OWN-SerC integrations with different noise strength  $\eta$  and parameter  $K$ . f) Similar to c) but showing the final value of the standard deviation of the phase shift  $\sigma_\phi$  for the OWN-SerC integrations. Parameters for the integrations are given in Table III. The standard deviation  $\sigma_\phi$  of the phase shift is high if coherence is low. The winding number remains zero if waves do not form as the integrations begin in a synchronous state. Non-zero winding number and low  $\sigma_\phi$  are typical of a coherent wave-state. Sufficiently high noise strength (that with  $\eta/K \sim 1$ , with division shown with dotted black lines) can cause the system to loose coherence by breaking into clusters of oscillators that move together. Asymmetric interactions ( $K_u/K \gtrsim 10$ , with division shown with dashed green lines) facilitate wave formation. Text labeling the lines are on the side of the line where coherent metachronal waves can exist.

### B. A modified overlap model with noise

To the directional model discussed in section IIIE (Eqn. 45), we add a Gaussian white noise term  $\xi_i(t)$  with strength  $\eta$  (with properties as discussed at the beginning

of section IV). The oscillator model is

$$\begin{aligned} \frac{d\theta_i}{dt} = & \omega_0 - \frac{\omega_0 K_u}{2} \left[ \tanh \left( \frac{\cos \theta_{i-1} - \cos \theta_i - \beta}{h} \right) + 1 \right] \\ & - K [\sin(\theta_i - \theta_{i+1}) + \sin(\theta_i - \theta_{i-1})] \\ & + \xi_i(t). \end{aligned} \quad (50)$$

The associated continuum equation is that of Eqn. 46 but with an additional white noise term

$$\begin{aligned} \theta_t = & \omega_0 - \frac{\omega_0 K_u}{2} \left[ \tanh\left(\frac{\beta}{h}\right) - 1 \right] + K dx^2 \theta_{xx} \\ & + \omega_0 K_u \text{sech}^2\left(\frac{\beta}{h}\right) \tanh\left(\frac{\beta}{h}\right) \frac{dx^2}{2h^2} [-(\theta_x)^2 + dx \theta_x \theta_{xx}] \\ & + \xi(x, t). \end{aligned} \quad (51)$$

In Figures 8a and b we show the final winding number and standard deviation  $\sigma_\phi$  of the series OWN-SerA of integrations where we vary the parameter  $K_u$  and the parameter  $K$  that diffusively stabilizes the model. Figures 8c and d are similar except they show the series OWN-SerB where we vary  $K_u$  and the noise strength  $\eta$ . Figures 8e and f are similar, except they show the series OWN-SerC where we vary  $K$  and the noise strength  $\eta$ . The integrations have parameters, including those held fixed, listed in Table III. On all panels in Figure 8 we show a dotted black line corresponding to  $\eta/K = 1$  and a dashed green or light green line showing  $K_u/K = 10$ .

Wave generation, giving positive winding number at the end of the integrations, is seen to the right of the dashed green line in Figure 8a and c and to the left of it in Figure 8e. Low values of  $K$  (diffusively preventing perturbations from growing) and high values of  $K_u$ , giving strongly asymmetric interaction, are required for wave generation, as seen in Figures 8a, c and e. With noise strength above  $\eta > K$  and if waves are generated, coherence is lost. This is seen in Figures 8b where the standard deviation of the phase shift  $\sigma_\phi$  is high below the  $\eta/K = 1$  line and in Figures 8d and f where  $\sigma_\phi$  is high above the  $\eta/K = 1$  line.

Figure 8 illustrates that given a particular noise strength, the parameters  $K$  and  $K_u$  of equation 50 can be adjusted to put the system in a region of parameter space that allows waves to form and remain coherent.

We find that clusters waves in a single direction tend to be generated for  $K_u/K > 10$ , independent of noise strength, with more coherent waves requiring larger values of  $K_u$ . These integrations have parameters  $h, \beta, \omega_0$  giving coefficient  $\bar{c}_{2a} \approx 27K_u$  (evaluated using Eqn. 35). The coefficient  $c_{1s} = 2K$  for this dynamical system. The  $K_u/K = 10$ , gives ratio  $\bar{c}_{2a}/c_{1s} = 135$ . Using the stability criterion of Eqn. 24, this gives a remarkably small phase shift of  $\phi \sim 0.4^\circ$ . So even though we found that Eqn 24 could predict the level of sinusoidal perturbations that cause instability (as discussed in section III E), if applied with a critical phase shift of order 1 radian, this criterion can underestimate the regime where noise can help drive clusters of waves in a single direction. In this respect, the stochastic directional model of Eqn. 50, considered here, is more sensitive to noise than the sinusoidal directional model of Eqn. 48, discussed in the previous section, Sec. IV A.

### C. Sensitivity of stochastic directional models to initial mean phase shift or slope

The integrations shown in Figures 6, 7, and 8 began with all oscillators set to zero, so the initial winding number, slope and mean phase shift are all zero. Because of the slope dependent diffusive term in the associated continuum equation, perturbations caused by noise can grow. The system increases or decreases in slope, depending upon the sign of  $\mu_{c+} - \mu_{c-}$  in the stochastic sinusoidal directional model of Eqn. 48, or the sign of  $K_u$  in the stochastic overlap model of Eqn. 50. What if the initial condition was a smooth ramp, so that the initial winding number and slope is non-zero? If the slope's sign allows perturbations to grow, then the integrations evolve, as shown in Figure 6, 7, and 8, until the system reaches a winding number and associated slope that is stable. However if the slope's sign is in the opposite direction, the system could remain sufficiently stable that the winding number would remain fixed. This would imply that the long-lived states of the stochastic models can be sensitive to initial conditions. To investigate this possibility we explore simulations with initial conditions that are linear ramps, with a single phase shift between neighboring oscillators.

In Figure 9 we show series of integrations for both stochastic models, denoted the DWN-SerW and OWN-SerW simulations, where we vary initial phase shift and noise strength. Initial conditions are ramped so that the phase shift between neighboring oscillators is fixed and determined from the initial winding number via Eqn. 14. In all panels we show on the top  $x$  axis the initial phase difference  $\phi_0$  in degrees. Parameters of the simulations are listed in Table III. In Figures 9a and c we show final winding number at the end of the integrations and in Figures 9a and c we show the standard deviation of the phase shifts,  $\sigma_\phi$ .

Positive slopes (corresponding to positive  $w_0$ ) are more stable for both sinusoidal stochastic model and stochastic overlap models shown in Figure 9. Figure 9a, showing the stochastic sinusoidal directional model, has a region on the lower right, with  $w_0$  ranging from 1 to 15, giving final winding number that is equal to the initial one. The region appears to have vertical bars with the same color. The region contains integrations that did not vary in winding number. Thus the integrations began in a stable state. With noise sufficiently strong (on the top right), variations in winding number occur, but at the expense of coherence in the resulting wave-like states, as seen in Figure 9b.

The stochastic overlap directional model has a similar region on the lower right in Figure 9c (with  $w_0$  ranging from 1 to 5) but it is much smaller than the stable region in Figure 9a. The stochastic overlap model is more sensitive to the growth of instabilities from noise than the sinusoidal stochastic directional model. For the sinusoidal model, the ratio  $c_{1s}/c_{2a}$  (derived from the stability criterion of Eqn. 24) corresponds to an unstable angle of

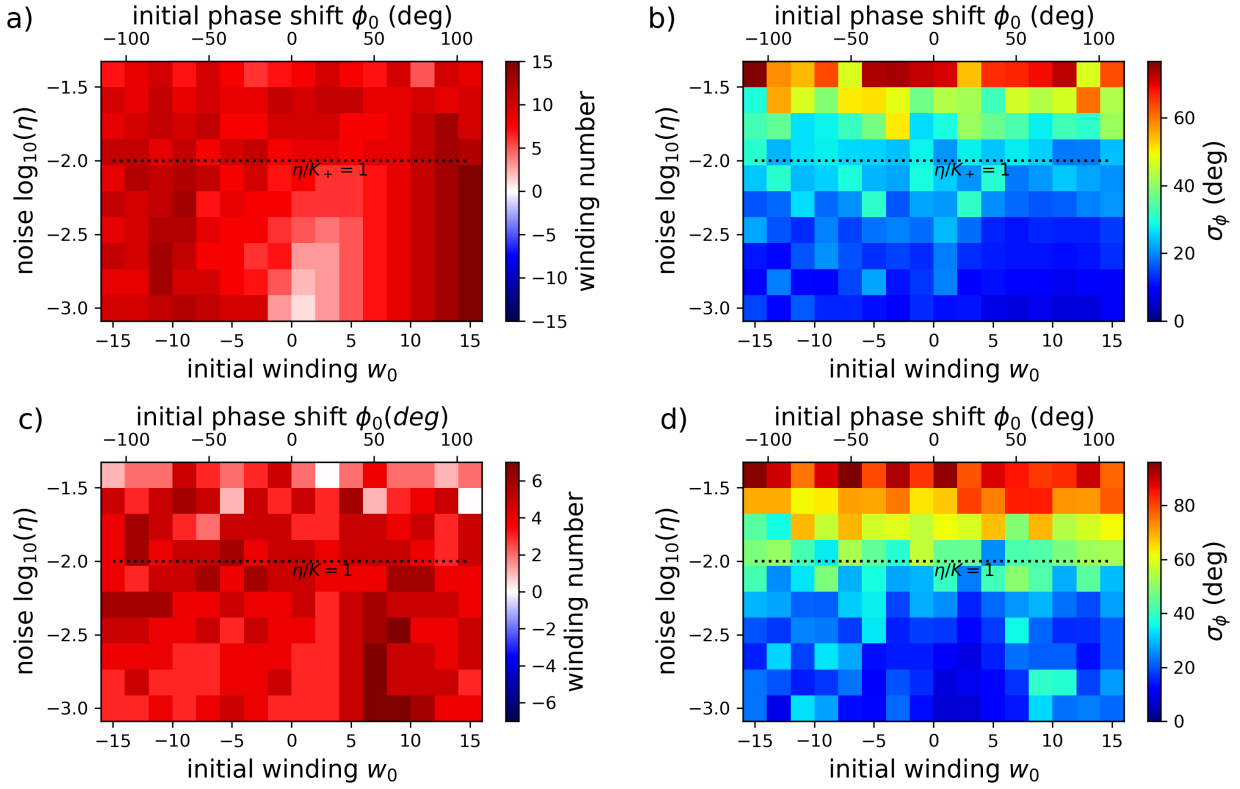


FIG. 9. Sensitivity of final winding number and standard deviation of phase difference to initial winding number  $w_0$  and noise strength  $\eta$ . Initial conditions have a constant slope with phase difference determined by the initial winding number. Parameters for each integration series are given in Table III. a) Final winding number is shown as a function of initial winding number  $w_0$  (on the  $x$  axis) and noise strength (on the  $y$  axis). Initial phase differences are shown in degrees on the top  $x$  axis. We show the DWN-SerW integration series which are for the stochastic sinusoidal directional model of Eqn. 48. b) The standard deviation of the phase difference at the end of the integrations also for the DWN-SerW integrations. c) Similar to a) but showing winding number for the OWN-SerW integrations. These are for the stochastic directional overlap model of Eqn. 50. d) Similar to b) but showing  $\sigma_\phi$  for the OWN-SerW integrations. For both models a positive initial slope can be stable, and the system would not exhibit variations in winding number, giving sensitivity of the final state to initial conditions. The regions where there are no changes in winding number have constant color in the vertical direction in panels a and c. For the stochastic directional overlap model (shown in panel c), the region where initial winding number is equal to the final one, on the lower middle right, is much smaller than for the stochastic sinusoidal directional model (shown in panel a). The stochastic overlap model is less sensitive to initial conditions and so more robustly gives metachronal wave states.

$19^\circ$ , whereas for the stochastic overlap model  $c_{1s}/c_{2a}$  is only  $0.2^\circ$ . The difference between these ratios could in part account for the different behavior of the two models. We increased the  $\mu_{c-}$  parameter in the sinusoidal stochastic model but we did not see the stable region in  $w_0$  significantly decrease in size. We suspect that the shape of the interaction functions influences their behavior and the criterion of Eqn. 24 is not sufficient to fully characterize the behavior of the stochastic models.

#### D. Sensitivity to the number of oscillators

Following [4, 17], the variance of the phases in a chain of interacting stochastic phase oscillators is predicted to depend on the number of oscillators in the system. The argument is based on the stochastic differential equation in Fourier space, that arises through linearizing the

Pardari-Parisi-Zhang equation (e.g., [30]), which arises in the continuum limit for the bidirectional model (as in Eqn. 22 or Eqn. 30 with the addition of noise). A long-wavelength cut-off arises from the number of oscillators  $N$  in a chain and this is predicted to cause the variance of the phases to depend upon the size of the system.

Is the mean phase shift in the directional models sensitive to the number of oscillators in a loop? To answer this question we ran three integration series where we vary the number of oscillators  $N$  and the strength of the noise  $\eta$ . The integrations parameters are listed in Table III and are shown in Figure 10. The number of oscillators integrated are powers of 2 ranging from 32 to 4096. The series are denoted DWN-SerN, for the directional sinusoidal model, the OWN-SerN, for the directional overlap model, and BWN-SerN for a bidirectional model that is same as the DWN-SerN, except the parameter setting asymmetry in the interactions  $\mu_{c-} = 0$ . Phases in these



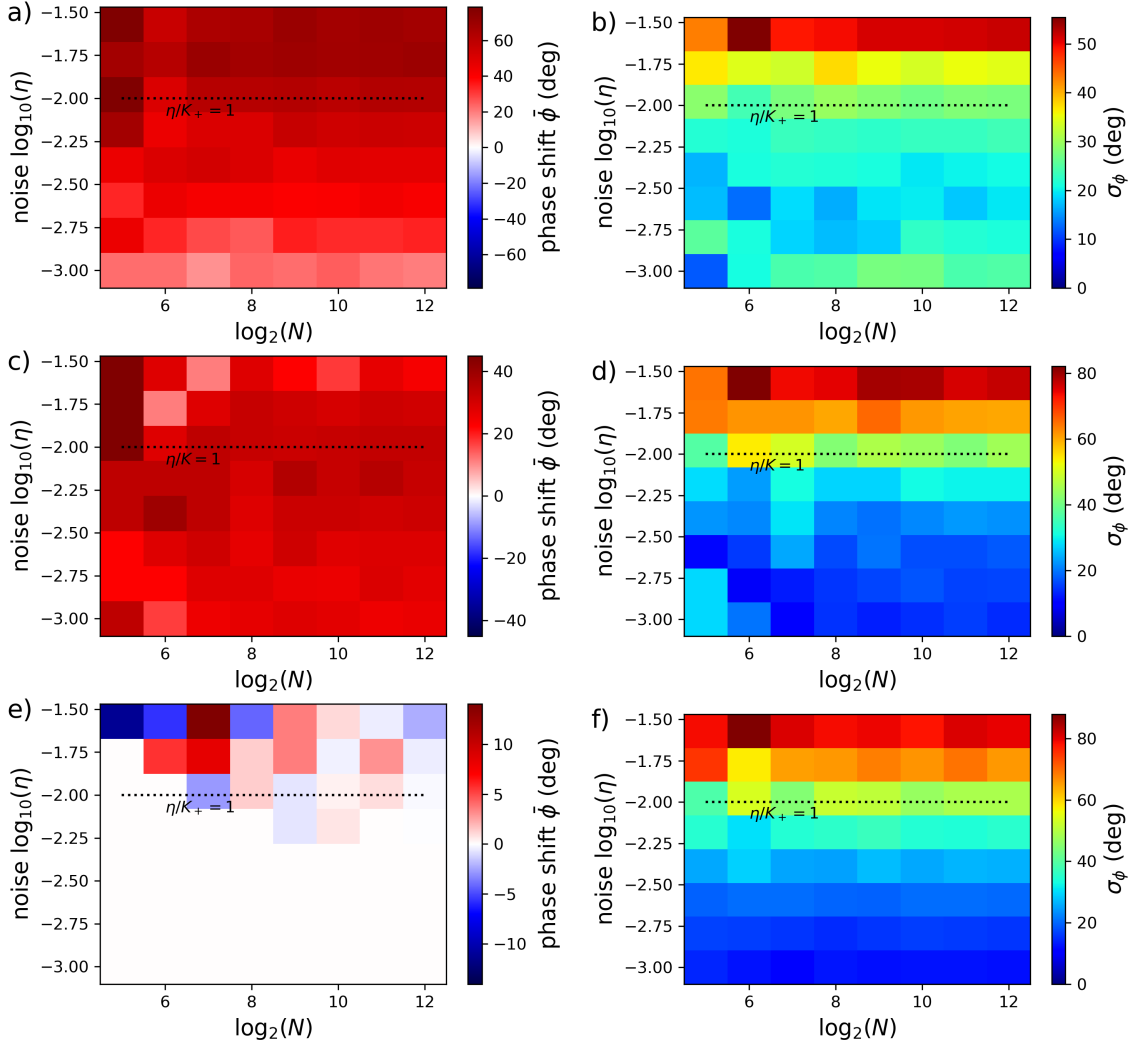


FIG. 10. Sensitivity of final mean phase shift and standard deviation of the phase shift to noise strength  $\eta$  and number of oscillators  $N$ . All phases are initially set to zero. Parameters for each integration series are given in Table III. a) Final mean phase shift  $\bar{\phi}$  is shown as a function of  $N$  (on the  $x$  axis) and noise strength (on the  $y$  axis). We show the DWN-SerN integration series which are for the stochastic sinusoidal directional model of Eqn. 48. b) The standard deviation of the phase difference at the end of the integrations also for the DWN-SerN integrations. c) Similar to a) but showing winding number for the OWN-SerN integrations. These are for the stochastic directional overlap model of Eqn. 50. d) Similar to b) but showing  $\sigma_\phi$  for the OWN-SerN integrations. e) Similar to a) but showing the BWN-SerN integrations which are of a bidirectional model. The parameters and model are the same as for the DWN-SerN integration, (shown in a) except the parameter giving asymmetry  $\mu_{c-} = 0$ . f) similar to b) except showing  $\sigma_\phi$  for the BWN-SerN integrations. In the directional models, we find that the mean and standard deviation of the phase shift,  $\bar{\phi}$  and  $\sigma_\phi$ , are insensitive to the number of oscillators in the loop.

integrations are initialized to zero. Instead of computing the winding number, which depends on  $N$ , we compute the mean phase shift  $\bar{\phi}$  (via Eqn. 14) at the end of each integration. The mean phase shifts  $\bar{\phi}$  are shown as images in Figures 10a,c,e and the standard deviations of the phase shifts  $\sigma_\phi$  are shown as images in Figures 10b,d,f.

Figures 10a,b,c,d shows that neither mean phase shift or standard deviation of the phase shift is sensitive to the number of oscillators in the loop for the directional stochastic models. We were curious whether this insensitivity is only a property of the directional models. Figure

10e and f shows a bidirectional model. The mean phase shift at the end of these integrations decreases with increasing  $N$ , which is opposite to what is expected if the mean phase shift scales with the phase variance which is predicted via Fourier analysis to be larger in a larger system in one-dimension. We consider explanations for this discrepancy. Our numerical investigations of section III found that variations in mean phase shift and winding number only occur when there are larger phase differences between neighboring oscillators. However, when the phase differences are large we do not expect the associated continuum equations to be good approximations

to the discrete models. Predictions based on the Kardar-Parisi-Zhang equation may be only be accurate in the discrete model before phase differences between oscillators become large. Possibly in addition, the term proportional to  $\theta_x \theta_{xx}$  in the associated stochastic continuum equation that is only present for directional models could give different behavior than predicted for the Kardar-Parisi-Zhang equation which lacks this term.

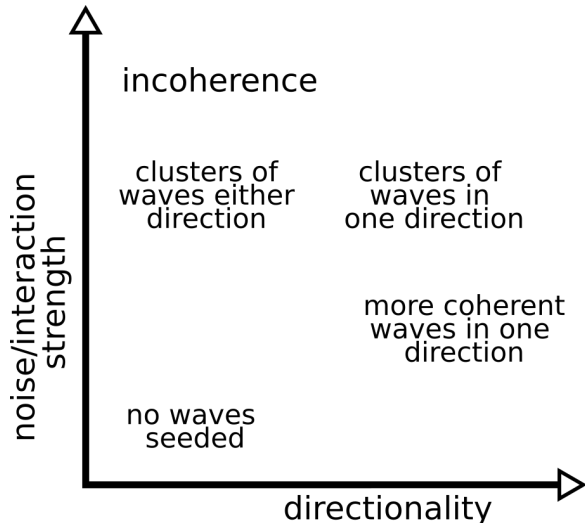


FIG. 11. Illustration of regimes for stochastic directional phase oscillator models.

## V. SUMMARY AND DISCUSSION

We have explored dynamical systems of chains of identical phase oscillators with nearest neighbor interactions that are arranged in a loop. We derive a continuum partial differential equation, accurate to third order in the separation between oscillators, that is a good approximation if phase differences are small. Numerical integrations and related continuum equations illustrate that directional models differ in some respects from bidirectional models (those with mirror reversal symmetry). We show a unidirectional model [12] that exhibits instability to small perturbations even for smooth initial conditions. The instability depends on the sign of the local slope and there is a preferred direction for emergent waves. The instability causes growth of short wavelength perturbations that grow to  $\pm\pi$  phase differences between neighboring oscillators. We attribute the instability to a third order diffusive term in the associated continuum partial differential equation that has sign that depends on the local slope. We also explore a bidirectional model [16] that only exhibits instabilities with initial conditions that contain large phase differences between neighboring oscillators.

In the continuum limit, and with a periodic boundary condition, winding number is like a topological charge

and is a conserved quantity [6]. We use numerical integrations of unidirectional and bidirectional discrete phase oscillator models with oscillators in a loop to find out whether and how winding number varies. We find that variations in winding number occur when there are groups of neighboring oscillators with phase differences near  $\pi$ . Variations in winding number cease after short wavelength perturbations decay. The resulting long-lived state is a synchronous or wave-like phase locked state with waves in either direction for the bidirectional model, but is a wave-like entrained state with a preferred direction in the unidirectional model.

The two lowest order diffusive terms ( $\propto \theta_{xx}$ ) in the associated continuum equations give a criterion for slope or phase shift dependent instability to the growth of small perturbations. With two phase oscillator models that let us adjust the directionality, we show that this criterion approximately predicts when small sinusoidal perturbations can grow and cause changes in winding number, resolving into metachronal waves.

With adjustable directional models we explored the role of white noise in influencing the states of these phase oscillator dynamical systems. An advantage of studying stochastic systems, is that the properties of long lived states could be insensitive to initial conditions. We find that as long as the strength of the noise does not destroy the coherence of the system (as previously noted by [17]), noise helps in developing and maintaining a wave-like state through seeding instabilities. The direction of the resulting waves is set by the asymmetry in the oscillator interaction functions. We support prior studies [17, 31] finding that directional models (lacking mirror symmetry in the oscillator interaction functions) are preferable for modeling phase oscillator systems that robustly enter and maintain a metachronal wave collective state.

We find that wave generation, as seen from the winding number during integrations that are initialized with zero phases, is sensitive to the strength of coefficients in the associated continuum equation, that depend upon derivatives of the oscillator interaction functions. However, in terms of ratios of these coefficients, the regions in parameter space where waves are found differed in the two directional stochastic models we explored.

We explored sensitivity of the stochastic directional models to initial conditions with a set slope or phase shift, corresponding to different initial winding numbers. Due to the directionality of these models, only smooth initial conditions with either positive or negative winding number can be stable. In the stable case, the final winding number can be set by the initial condition. The range of possible winding numbers (or initial phase shifts) where long-lived wave-like states depend upon the initial phase shift depends upon the oscillator interaction functions. With the stochastic bidirectional overlap model we explored, the region where winding number is set by the initial slope is much smaller than for the stochastic sinusoidal directional model. This suggests that stochastic models with strong directionality would more robustly

enter metachronal wave states and would be less sensitive to initial conditions.

We explored sensitivity of the stochastic directional models to the number of oscillators in the loop. Contrary to expectations based on Fourier analysis of stochastic continuum equations [4, 17], we find that mean phase shift and the standard deviation of the phase shift, after integration, are insensitive to the number of oscillators. The scaling estimated via Fourier analysis may fail because the continuum equation is a poor approximation to the discrete interacting oscillator chain models when phase differences between neighboring oscillators are large.

Given a particular level of noise, is it possible to choose phase oscillator interaction functions that would robustly give long-lived metachronal wave states? Based on our exploration of two bidirectional models, we roughly illustrate regimes of collective behavior in Figure 11. Because noise seeds perturbations that can cause variations in winding number, the strength of the symmetric interactions must not be so strong that perturbations are damped rapidly. For waves to be formed, the strength of the directionality, set by asymmetry in the interactions, should be sufficiently strong that small perturbations are unstable and can grow to large enough values to change the winding number. The interaction strengths cannot be so weak that noise causes generated waves to completely lose coherence. With sufficiently strong asymmetric interactions, we suspect that a stochastic model is relatively insensitive to initial conditions, in the sense that only for a small range of smooth and sloped initial conditions would the system's long-lived states depend upon the initial slope. Most of our integrations of stochastic directional models exhibited clusters of oscillators in wave-like states, but with waves in a particular direction, rather than a coherent wave that spanned the entire system. If metachronal waves in biological systems rely on noise to seed waves, then there might be a trade-off between wave coherence and sensitivity to initial conditions. Robustly generated states consisting of clusters of oscillators driving waves, may be functionally preferable to unreliably generated but coherent wave states.

Future study could improve upon our understanding of how the characteristics of the interaction functions and the nature of stochastic perturbations affect wave-generation (as seen from statistics of the winding number or mean phase shift), the coherence of the generated waves and the sensitivity to initial conditions. In biological systems, statistics of wave speeds, variations in wave speed and coherence of clusters of oscillators showing coherent phase shifts, might pin down the role of noise in seeding and maintaining metachronal wave states and better constrain the nature of interactions between the oscillators.

For the models we explored, large phase differences led to instability which resolved with changes in winding number. Using a perturbative analysis and by computing eigenvalues of a circulant matrix, Niedermayer et al. [16]

shows explicitly for their bidirectional model (Eqn. 27) that a phase locked state with a phase shift above  $\pi/2$  between each oscillators would be unstable. It is more difficult to similarly assess (via a perturbative linear analysis) the stability of an entrained state with a large phase shift in the unidirectional model (Eqn. 31) because this requires averaging over the oscillation period of the entrained state. Instability when the phase differences are large is not necessarily sufficient for robust formation of waves. To form waves in particular direction, jumps in phase should resolve in a particular direction. In other words, the phase difference should preferentially cross  $\pi$  in either the clockwise or counter clockwise direction (as is true for our unidirectional model but not the bidirectional model) to ensure that waves form moving in a specific direction. Perhaps insight can be sought by studying propagation of phase kinks in other settings (e.g., [32]).

We gained intuition by looking at the partial differential equation that approximates an oscillator chain model. However the continuum equations, which are derived in the limit of small phase shift, do not help us predict how jumps in phase evolve. We have noticed that a single large jump in phase is not sufficient to cause a change in winding number, rather at least two large phase jumps in sequence are required. If the collective behavior of the model is sensitive to the dynamics of strong short wavelength perturbations, then desirable models for actual biological systems should be good approximations in both short and long wavelength limits. The interaction functions for the models we have explored do not contain more than one minimum or maximum. There may be constraints on the shapes of the periodic functions that permit changes in winding number in the associated phase oscillator dynamical systems.

The partial differential equation that approximates a directional oscillator chain model in the continuum limit resembles the Kardar-Parisi-Zhang equation but with the addition of a third order non-linear term that is proportional to  $\theta_x \theta_{xx}$ . The slope dependent instability we see in the discrete models suggests that the stochastic version of this differential equation may exhibit novel phenomena that is not present with the Kardar-Parisi-Zhang equation.

Hydrodynamic interaction models for cilia can be directional (e.g., [6, 17]). We have shown here that there are directional models that exhibit changes in winding number, but that does not necessarily mean that this class of models is appropriate for real biological systems. Quantitative measurements describing the coherence of generated waves may help differentiate between stochastic models. By evaluating the strength and shape of the symmetric and antisymmetric hydrodynamic interaction functions for cilia it may be possible to determine if instabilities mediate changes in the winding number so that these systems can preferentially enter and maintain sufficiently coherent wave-like states. If this is not the case, then alternate physical mechanisms are required to account for the formation of metachronal waves. For

example, physical gaps in ciliated systems, which relax the constraint of a periodic boundary condition, could facilitate metachronal wave formation, as proposed by Chakrabarti et al. [6]. Additional physical mechanisms for oscillator interaction [33], variations in properties and additional degrees of freedom describing the individual oscillators could influence the collective behavior of these

interacting systems.

## ACKNOWLEDGMENTS

We thank Nathan Skerrett and Brato Chakrabarti for helpful discussions.

- 
- [1] N. Wiener, *Nonlinear Problems in Random Theory* (MIT Press, Cambridge, MA, 1958).
  - [2] Y. Kuramoto, in *Int. Symposium on Mathematical Problems in Theoretical Physics*, edited by H. Araki (Springer, 1975), vol. 39 of *Lecture Notes in Physics*, pp. 420–422.
  - [3] Y. Kuramoto and I. Nishikawa, *Journal of Statistical Physics* **49**, 569 (1987), URL <https://doi.org/10.1007/2Fb01009349>.
  - [4] A. Pikovsky, J. Kurths, M. Rosenblum, and J. Kurths, *Synchronization: a universal concept in non-linear sciences*, 12, no. 12 in Cambridge Nonlinear Science Series (Cambridge university press, 2003).
  - [5] S. Strogatz, *Sync: How Order Emerges From Chaos In the Universe, Nature, and Daily Life* (Hachette Books, 2012), ISBN 9781401304461, URL <https://books.google.com/books?id=vHw44RSi0CwC>.
  - [6] B. Chakrabarti, S. Furchauer, and M. J. Shelley, *Proceedings of the National Academy of Sciences* **119**, e2113539119 (2022).
  - [7] S. L. Tamm, *The Journal of Cell Biology* **55**, 250 (1972).
  - [8] M. A. Sleight, J. R. Blake, and N. Liron, *American Review of Respiratory Disease* **137**, 726 (1988).
  - [9] B. A. Afzelius, *Journal of Pathology* **204**, 470 (2004).
  - [10] R. Faubel, C. Westendorf, E. Bodenschatz, and G. Eichele, *Science* **353**, 176 (2016).
  - [11] A. Peshkov, S. McGaffigan, and A. C. Quillen, *Soft Matter* **18**, 1174 (2022).
  - [12] A. C. Quillen, A. Peshkov, E. Wright, and S. McGaffigan, *Phys. Rev. E* **104**, 014412 (2021).
  - [13] D. A. Wiley, S. H. Strogatz, and M. Girvan, *Chaos* **16**, 015103 (2006).
  - [14] P. F. C. Tilles, F. F. Ferreira, and H. A. Cerdeira, *Physical Review E* **83** (2011), URL <https://doi.org/10.1103/2Fphysreve.83.066206>.
  - [15] K. Dénes, B. Sándor, and Z. Neda, *Communications in Nonlinear Science and Numerical Simulation* **78**, 104868 (2019), ISSN 1007-5704, URL <http://www.sciencedirect.com/science/article/pii/S1007570419301881>.
  - [16] T. Niedermayer, B. Eckhardt, and P. Lenz, *Chaos: An Interdisciplinary Journal of Nonlinear Science* **18**, 037128 (2008), URL <https://doi.org/10.1063/2F1.2956984>.
  - [17] A. Solovev and B. M. Friedrich, *Chaos* **32**, 013124 (2022).
  - [18] D. R. Brumley, M. Polin, T. J. Pedley, and R. E. Goldstein, *Physics Review Letters* **109**, 268102 (2012).
  - [19] R. Ma, G. Klindt, I. Riedel-Kruse, F. Jülicher, and B. Friedrich, *Phys Rev Lett.* **113**, 048101 (2014).
  - [20] J. A. Acebron, L. L. Bonilla, C. J. P. Vicente, F. Ritort, and R. Spigler, *Reviews of Modern Physics* **77**, 137 (2005).
  - [21] G. Ermentrout and N. Kopell, *Comm. Pure Appl. Math.* **49**, 623 (1986).
  - [22] G. Ermentrout and N. Kopell, *SIAM J. Appl. Math.* **50**, 1014 (1990).
  - [23] L. Ren and B. Ermentrout, *Physica D: Nonlinear Phenomena* **143**, 56 (2000), URL <https://doi.org/10.1016/2Fs0167-2789%2800%2900096-8>.
  - [24] J. Elgeti and G. Gompper, *PNAS; Proceedings of the National Academy of Sciences* **110**, 4470 (2013).
  - [25] P. Muruganandam, F. F. Ferreira, H. F. El-Nashar, and H. A. Cerdeira, *Pramana* **70**, 1143 (2008), URL <https://doi.org/10.1007/2Fs12043-008-0119-8>.
  - [26] D. Aeyels and J. A. Rogge, *Progress of Theoretical Physics* **112**, 921 (2004).
  - [27] Z. Zheng, G. Hu, and B. Hu, *Phys. Rev. Lett.* **81**, 5318 (1998).
  - [28] B. Ottino-Löffler and S. H. Strogatz, *Physical Review E* **94** (2016), URL <https://doi.org/10.1103/2Fphysreve.94.062203>.
  - [29] M. Cross and H. Greenside, *Pattern Formation and Dynamics in Nonequilibrium Systems* (Cambridge Univ. Press, Cambridge, U. K., 2009).
  - [30] A.-L. Barabási and H. E. Stanley, *Fractal Concepts in Surface Growth* (Cambridge University Press, Cambridge, 1995).
  - [31] A. Solovev and B. M. Friedrich, *New Journal of Physics* **24**, 013015 (2022).
  - [32] H. Chaté, A. Pikovsky, and O. Rudzick, *Physica D* **131**, 17 (1999).
  - [33] N. Narembatsu, R. Quek, K.-H. Chiam, and Y. Iwadate, *Cytoskeleton* **72**, 633 (2015).